



# Genetic circuit design automation for yeast

Ye Chen<sup>1</sup>, Shuyi Zhang<sup>1</sup>, Eric M. Young<sup>1</sup>, Timothy S. Jones<sup>2</sup>, Douglas Densmore<sup>2</sup> and Christopher A. Voigt<sup>1</sup>✉

**Cells can be programmed to monitor and react to their environment using genetic circuits. Design automation software maps a desired circuit function to a DNA sequence, a process that requires units of gene regulation (gates) that are simple to connect and behave predictably. This poses a challenge for eukaryotes due to their complex mechanisms of transcription and translation. To this end, we have developed gates for yeast (*Saccharomyces cerevisiae*) that are connected using RNA polymerase flux as the signal carrier and are insulated from each other and host regulation. They are based on minimal constitutive promoters (~120 base pairs), for which rules are developed to insert operators for DNA-binding proteins. Using this approach, we constructed nine NOT/NOR gates with nearly identical response functions and 400-fold dynamic range. In circuits, they are transcriptionally insulated from each other by placing ribozymes downstream of terminators to block nuclear export of messenger RNAs resulting from RNA polymerase readthrough. Based on these gates, Cello 2.0 was used to build circuits with up to 11 regulatory proteins. A simple dynamic model predicts the circuit response over days. Genetic circuit design automation for eukaryotes simplifies the construction of regulatory networks as part of cellular engineering projects, whether it be to stage processes during bioproduction, serve as environmental sentinels or guide living therapeutics.**

Yeast engineering projects often require programming the cell to do different things at different times. For example, cells could create hierachal structures as they grow into living materials or work together during fermentation to build a complex product<sup>1–6</sup>. Progress has been made in building circuits in *Saccharomyces cerevisiae*, including logic gates and memory<sup>1,7–22</sup>. However, building such circuits requires specialized expertise and, while often qualitatively guided by mathematical models, the mapping of a function to a DNA sequence is a slow trial-and-error process<sup>1,7,23–26</sup>. Cello is design automation software that seeks to empower engineers to incorporate circuits into their projects, while abstracting them from the details of designing the DNA sequence. A user specifies the circuit function using a species-independent language (Verilog), which is mapped by the software to a particular species using data in a user constraint file (UCF) (Fig. 1). The UCF also defines the location of the circuit, the gates and mathematical model used to connect them, and composition rules for the DNA sequence. To date, UCFs have been built for the prokaryotes *Escherichia coli* DH10β (p15a plasmid) and *Bacteroides thetaiotaomicron* (genome), but have not been developed for a eukaryote<sup>27–29</sup>.

NOR gates are simple to implement and can be connected to build any circuit function<sup>24,30,31</sup>. They have two input promoters that express a repressor that turns off an output promoter. The signal connecting the gates is the RNA polymerase (RNAP) flux emanating from the promoters. The response function of a gate captures how the output changes as a function of the input(s) and is used by mathematical models to predict how gates can be combined to build a circuit<sup>27</sup>. Measuring RNAP flux directly is difficult, so the promoter activities are compared with a reference promoter and reported in relative promoter units (RPUs)<sup>32,33</sup>.

The precision of design automation software is only as good as the gate technology. Gates must generate the same response in the context of different circuits. For prokaryotic gates, context dependence has been reduced using insulators based on ribozymes, long promoters and strong terminators<sup>25,34–38</sup>. Eukaryotic regulation is more complex and difficult to insulate. Promoter strength can be

impacted by global chromosome structure, nucleosome occupancy, pervasive transcription and interactions with the nuclear pore complex<sup>39–46</sup>. Chromosomes have natural mechanisms of insulation but their function cannot be reduced to a discrete genetic part<sup>47–50</sup>. Native promoters are usually sensitive to environmental conditions and genetic context, and this sensitivity is retained when they are used as scaffolds to insert operators to make them regulatable<sup>1,42,47,51–55</sup>. To address these issues, minimal promoters have been designed<sup>42,52,56–58</sup>. Neighbouring transcription units can also influence each other by affecting nucleosome repositioning<sup>59–62</sup>. It has been found that T-rich promoters lead to nucleosome-free regions, thus resulting in strong promoters with reduced noise that are less impacted by neighbouring DNA<sup>40,57,62–66</sup>. Promoters can also be affected by the downstream terminator because it can re-initiate RNAP<sup>46,57,67–75</sup>. This can also make the use of terminators to separate transcription units problematic<sup>76,77</sup>. To insulate against chromatin structure, Klavins and co-workers<sup>24</sup> developed CRISPR interference (CRISPRi)-based gates where dCas9 is fused to a chromatin remodelling domain.

Here, we designed short synthetic promoters that are <120 base pairs (bp) and can be strongly repressed. These were used to build three sensors and nine NOT/NOR gates using prokaryotic DNA-binding proteins. The rules for operator placement were developed based on a 20-T spacer that is diversified to avoid homologous recombination. These gates have near-identical response functions with up to 100-fold dynamic range and low basal transcription. The gate thresholds were tuned to be similar through the selection of Kozak sequences. The gates were integrated into the chromosome, their response functions characterized and the data used to build a UCF for *S. cerevisiae* BY4741 (SC1C1G1T1). Cello 2.0 was then used to design large genetic circuits (up to 33,000 bp and 11 regulatory proteins) (Fig. 1). The sensors were always located at the NRT1 locus (I.ChXV)<sup>78</sup> and the circuits were divided between two loci (IIA.ChIII and IIB.ChV) (Supplementary Fig. 1)<sup>79–81</sup>. New insulators were specified to occur in a defined order, between which the gates were positioned. A dynamic model, parameterized by the responses of individual gates, is able to predict the circuit response over weeks.

<sup>1</sup>Synthetic Biology Center, Department of Biological Engineering, Massachusetts Institute of Technology, Cambridge, MA, USA. <sup>2</sup>Department of Electrical and Computer Engineering, Boston University, Boston, MA, USA. ✉e-mail: cavoigt@gmail.com

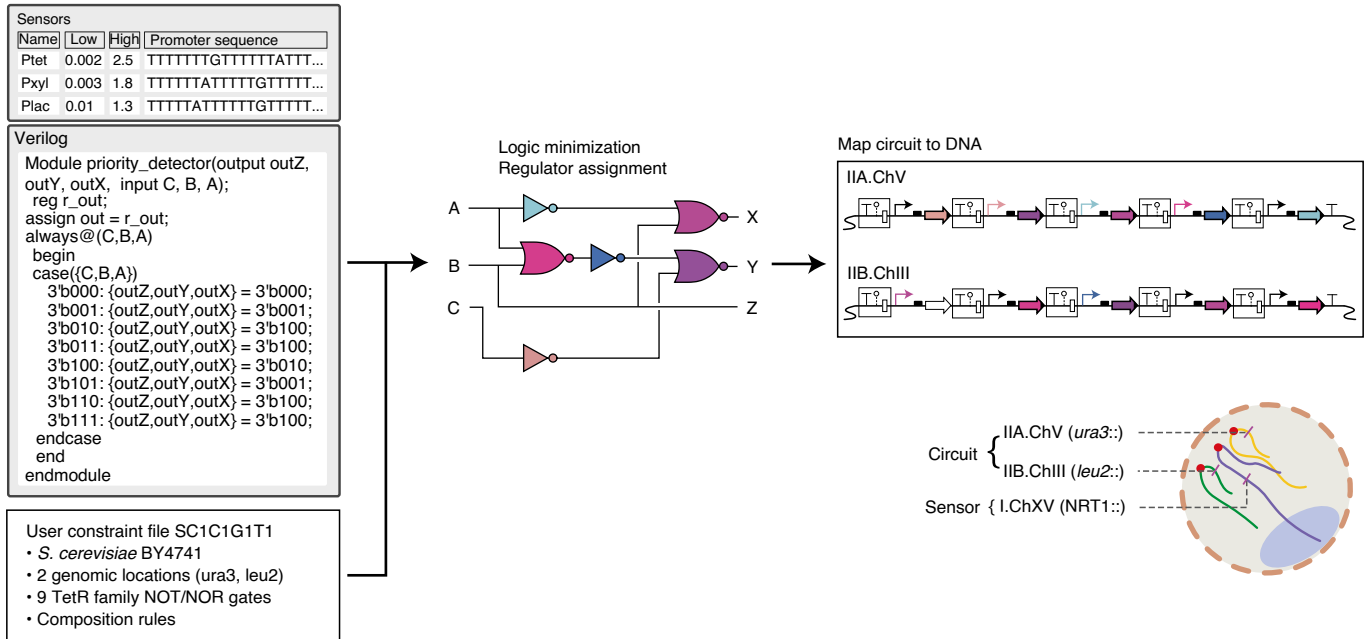


**Fig. 1 | *S. cerevisiae* circuit design using Cello 2.0.** The sensors A, B and C, Verilog code for the circuit and UCF are defined. Cello 2.0 parses the Verilog text, uses logic minimization to create a wiring diagram and simulated annealing to assign repressors to each gate (colours). Finally, the composition rules are used to map the circuit to a DNA sequence. The illustration of the chromosomes was derived from ref. <sup>81</sup>.

## Results

**Genetic parts to build insulated gates.** NOT/NOR gates are based on a strong promoter that is turned off by a repressor. This promoter must not be sensitive to environmental or growth conditions. To this end, we designed synthetic constitutive promoters based on a TATA box and 20-bp transcription start site (TSS) gleaned from the *ADH2* gene (Fig. 2a)<sup>62,82,83</sup>. We varied the location and sequences of the upstream activating sequence (UAS) and region between the TATA box and TSS (Extended Data Fig. 1). From these, we selected a promoter based on Gal4-binding UAS sites flanked by two 15-bp poly-T sequences and a 31-bp spacer between the UAS and TATA box from the Gal1 promoter. This scaffold was used to determine how best to insert operators. Either one or two *tetO*<sub>2</sub> operators were placed at different locations (Fig. 2b) (repeated for *lacI/lacO*; Extended Data Fig. 2). The promoters were fused to a 10-bp Kozak sequence and the yellow fluorescent protein gene (*yfp*) and cloned into a plasmid (Supplementary Fig. 15). TetR containing a nuclear localization signal (NLS)<sup>84</sup> was constitutively expressed from a second plasmid (Supplementary Fig. 15). Fluorescence measurements were made using strains carrying the promoter reporter in the presence or absence of the plasmid expressing TetR (Fig. 2b) (Methods). The strongest repression was consistently observed for promoters containing two operators separated by more than 20 bp.

To eliminate Gal4 as a regulatory input, we identified an alternative UAS that could achieve high expression levels. We found that a 20-bp poly-T sequence separated from the TATA box by 4 bp consistently led to a strong promoter that was independent of whether cells were grown in glucose or galactose (Extended Data Fig. 1). The Kozak sequence was shortened to only 10 bp (Supplementary Table 6)<sup>85</sup>. Collectively, these changes led to a short (<120 bp) canonical promoter structure (Psyn.0ac) (Fig. 2a).

A repressor set was then collated, including LacI, XylR, LexA, as well as a set of TetR family repressors and bacteriophage repressors (CI, CI434 and HKCI), from which we eliminated those that were toxic or exhibited crosstalk (not shown)<sup>1,23,25,86–88</sup>. Based on the Psyn.0ac scaffold, we designed a set of promoters that can respond

to 12 repressors (Extended Data Fig. 1 and Supplementary Figs. 2–12). For those repressors used to build gates, two variants of each promoter were built so that they could be used without invoking homologous recombination (Fig. 2c).

Readthrough of RNAP from a gate to its neighbours can cause circuit failures<sup>89</sup>. To block transcription between gates, 33 yeast terminators were characterized downstream from 35 promoters (Fig. 3a and Supplementary Tables 7 and 8) (Methods). All 1,155 combinations were evaluated and, while there were some outliers, we found that the expression level was dominated by promoter choice (Fig. 3a).

When terminators appear immediately adjacent to a promoter, they can change the nucleosome occupancy and promoter activity<sup>76</sup>. Spacers were identified to disrupt this effect that are based on ribozymes (RiboJ variants<sup>35,90,91</sup>) placed between the terminator and promoter. While this does not stop an errant transcript from being produced, it is cleaved and not capped or exported from the nucleus, thereby blocking expression. When a ribozyme was placed after an inducible promoter and before a reporter gene, induction no longer led to expression (Fig. 3b and Supplementary Fig. 15). Insulators were then constructed by pairing the strongest terminators with a ribozyme and spacer, and evaluated in the genome for their ability to stop an upstream inducible system (Van) from influencing a neighbouring inducible system (anhydrotetracycline hydrochloride (aTc)) (Fig. 3c and Extended Data Fig. 3). All of the insulators were able to block interference, thus enabling the two neighbouring inducible systems to function independently.

**Definition of a reference promoter.** Several reference promoters have been defined for *E. coli* and used to report promoter activities in RPUs<sup>32,33</sup>. To define a similar reference promoter for *S. cerevisiae*, we selected PFY1 based on an analysis by Ellis and co-workers<sup>11</sup> demonstrating that it is the least affected natural constitutive promoter when cells are grown in diverse conditions. Like them, we inserted it into the *ura3* locus, but flanked it by strong terminators and an upstream ribozyme to buffer against transcriptional

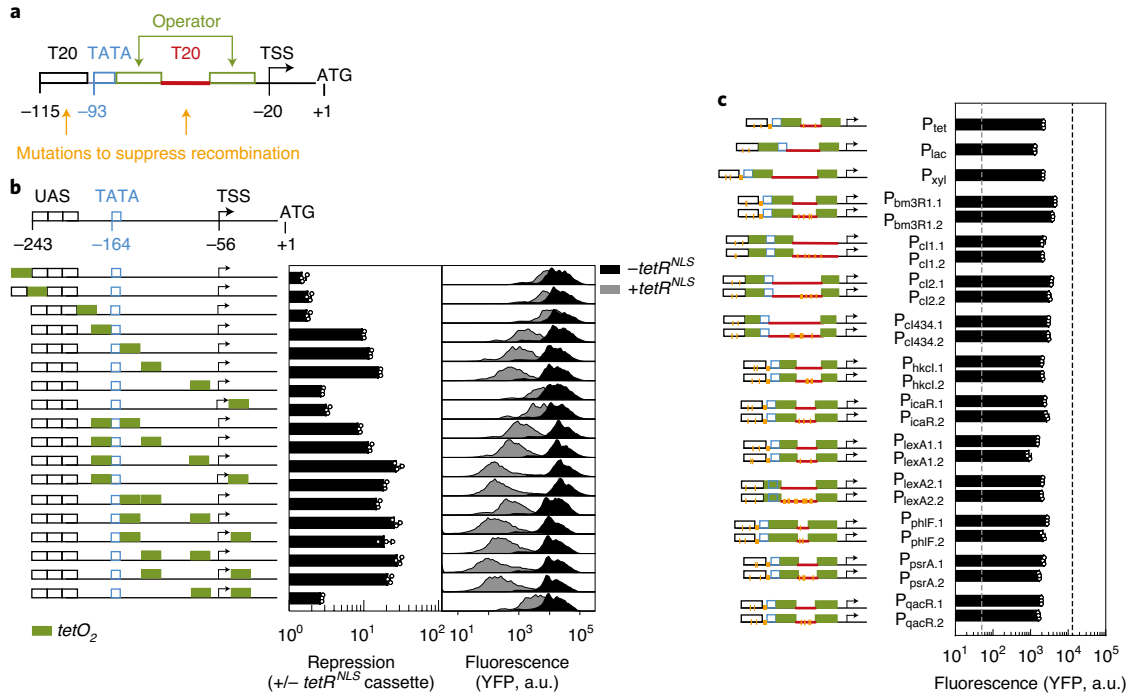


**Fig. 2 | Design of minimal synthetic promoters that respond to regulators.** **a**, The canonical promoter design is shown. The TATA box (blue) is TATAAAA. Sequences consisting of 20 T nucleotides are placed upstream of the TATA box and between the operators. Mutations are made to these sequences to avoid recombination. The TSS region is sourced from 20 bp from the native ADH promoter, and the Kozak sequence is a synthetic 10-bp sequence<sup>85</sup>. All genetic parts are provided in Supplementary Tables 5, 7 and 8. **b**, Comparison of operator spacing. The promoter backbone is Psyn.0 with a Gal4 UAS (Supplementary Fig. 2) and is cloned into a reporter plasmid (Supplementary Fig. 15). A second plasmid is constructed from which TetR is expressed from a constitutive promoter (Supplementary Fig. 15). The cytometry distributions show the fluorescence from the reporter plasmid in the absence (black) and presence (grey) of the TetR plasmid, and the fold-change is the ratio of the median of these distributions. **c**, The architectures of the final synthetic promoters and their strengths are shown. The colours correspond to **a**. The sequences are provided in Supplementary Table 5 and the promoters were integrated into the IIA.ChV (sensor promoters) or IIB.ChIII genomic loci (gate promoters). The step-by-step design of each promoter is described in Extended Data Fig. 1 and Supplementary Figs. 2–12. The mutations made to diversify the stretches of T nucleotides are shown as vertical orange lines; two promoters were selected to be used in gates (and one for those used in sensors). The lower dashed line marks the fluorescence of white cells and the upper dashed line is the strong P<sub>TDH3</sub> promoter. a.u., arbitrary units. In all parts, the data represent the average of three experiments performed on different days.

readthrough from the genome (*S. cerevisiae* CY671int) (Fig. 4a). The fluorescence was measured by cytometry and defined as 1 RPU (Fig. 4b and Extended Data Fig. 4).

**Design of sensors and gates.** A sensor array was constructed at the I.ChXV locus, from which regulatory proteins for three small molecule sensors were expressed (Fig. 4c). The xylose sensor is based on XylR from *Bacillus licheniformis*, which we identified from libraries of regulatory proteins and promoters (Supplementary Fig. 13). Three strains were constructed to measure the output promoter of each sensor integrated into IIA. ChV. The aTc, isopropyl β-D-1-thiogalactopyranoside (IPTG) and xylose sensors generated 1,200-fold, 120-fold and 600-fold induction, respectively (Fig. 4d and Extended Data Fig. 5). The sensors showed no cross-reactivity with respect to each other's small molecules (Fig. 4e).

We constructed nine NOT gates based on the repressors and their cognate minimal promoters. The input to the gates was the IPTG-inducible P<sub>lac</sub> promoter (Fig. 5a). The gate was encoded at IIA. ChV and the output promoter transcribing yfp was integrated at IIB. ChIII. The gate was turned off by adding IPTG, but if the x-axis of the response function was presented in units of concentration, it could not be used to calculate how to connect the gate to a different input promoter. To address this, we constructed a separate strain to measure the P<sub>lac</sub> response to IPTG and then used these data

to convert the x-axes of the response functions to RPUs (Extended Data Fig. 6), which were then fit to:

$$y(x) = y_{\min} + \frac{(y_{\max} - y_{\min})K^n}{K^n + x^n} \quad (1)$$

The resulting fits are shown in Fig. 5b and parameters are shown in Supplementary Table 2 (see also Extended Data Figs. 7 and 8). We selected Kozak sequences and output promoters to generate similar response functions. The ranges of  $y_{\min} \in [0.001, 0.2]$  and  $y_{\max} \in [1.5, 5.1]$  spanned the response threshold of the gates (~1 RPU), thus making them easier to connect. To test whether the repressors were orthogonal, we built  $9 \times 9 = 81$  strains that varied the repressor expressed from IIA. ChV and the output promoter carried in IIB. ChIII, and no cross-reactions were observed (Fig. 5c). Finally, the growth impact of each gate was measured as a function of the strength of the input promoter (Extended Data Figs. 7 and 8). These data were used by Cello 2.0 to predict the growth impact of the circuit, and the algorithm avoided toxic combinations. Cl434 and QacR slowed growth before reaching maximum repression and were therefore avoided by the algorithm.

The gate dynamics were quantified using a simple model that captured the characteristic times ( $\tau_{\text{ON}}$  and  $\tau_{\text{OFF}}$ ) for a gate to switch OFF → ON or ON → OFF (Methods)<sup>28</sup>. To perform these measurements, strains were grown under one set of conditions (with

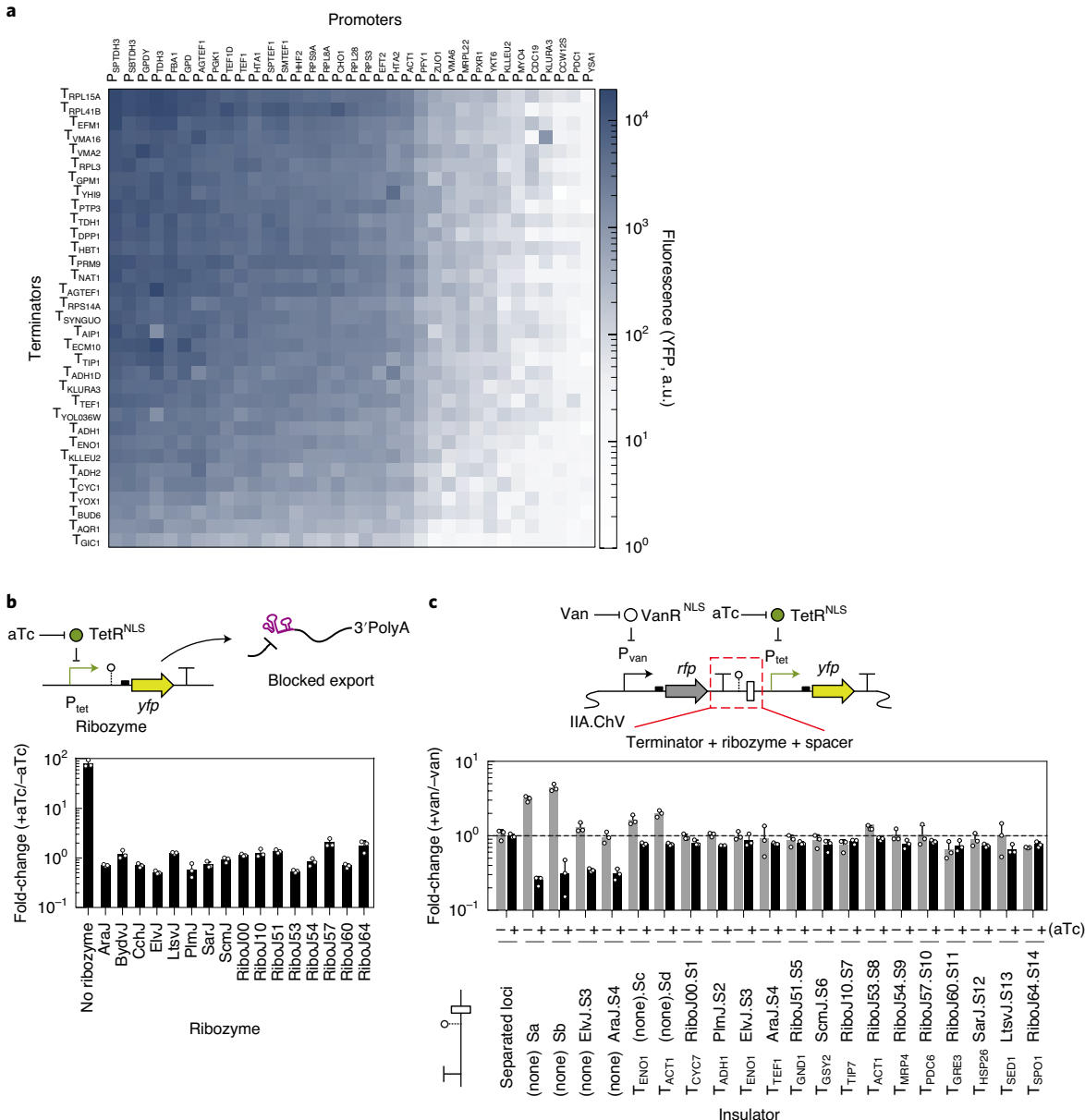


**Fig. 3 | *S. cerevisiae* terminator and insulators. a, All combinations of promoters and terminators were tested for their ability to express a YFP reporter when grown in media containing glucose (Methods and Supplementary Fig. 16). Note that these measurements were made in a different strain background (*S. cerevisiae* CENPK.113-7D) than the remainder of the experiments in this manuscript. The grid represents single data points taken during the screen. The DNA sequences of the promoters and terminators are provided in Supplementary Tables 7 and 8, respectively. b, Evaluation of ribozyme activity in blocking mRNA export. The ribozyme is placed after an aTc-inducible promoter and before the *yfp* reporter on a plasmid (Supplementary Fig. 15). The fold-change of the fluorescence is shown as the ratio in the presence and absence of 100 ng ml<sup>-1</sup> aTc. These data represent the average of three experiments performed on different days. c, Measurement of readthrough between two adjacent transcription units. Different terminator/ribozyme/spacer combinations were tested using the system shown (the grey gene is *rfp*, but this was only used as a spacer). The bars show the ratio of *yfp* fluorescence measured upon induction of the upstream sensor ( $\pm$ 200  $\mu$ M vanillic acid). Two transcription units were also integrated into different chromosomes (IIA.ChV and IIB.ChIII) for comparison (separated loci). Two 450-bp nonfunctional DNA spacer sequences (S1 and S2) were chosen as a control for the absence of an insulator. In all parts, the data represent the average of three experiments performed on different days.**

or without inducer) until reaching steady state. Then, they were transferred into fresh media with the opposite conditions (Methods and Extended Data Figs. 7 and 8). These data were fit to differential equation models to calculate  $\tau_{\text{ON}}$  and  $\tau_{\text{OFF}}$  (Supplementary Table 2). Note that the times required for inducer to be taken up by the cells and YFP to express and fold were separated from these values.

A NOR gate architecture was developed for the *S. cerevisiae* genome (Fig. 5d). Two copies of the repressor gene were designed

with different codon usages. Each gene was paired with the same Kozak sequences and was driven by input promoter 1 or 2. To test this NOR gate design, we used the IcaR repressor and the aTc and IPTG sensors (Fig. 5e). The gate produced the expected two-dimensional NOR response function (Fig. 5f) independent of whether the copies of the repressor genes were co-located (Fig. 5g). It is simpler for Cello to compute how to connect gates if the NOR gate response function can be described as a one-dimensional

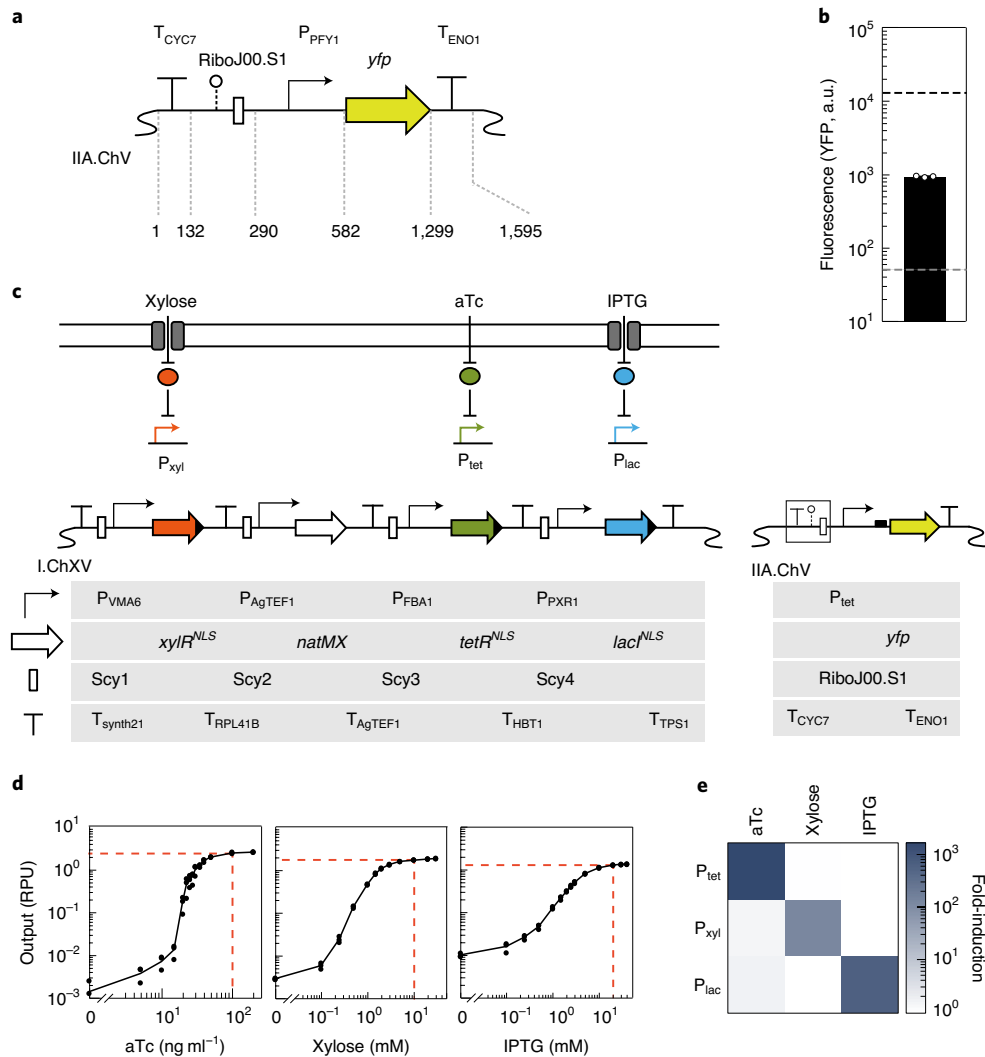


**Fig. 4 | Small molecule sensors.** **a**, The RPU reference promoter is shown. The DNA sequence is provided in Supplementary Table 11. **b**, The arbitrary units of fluorescence were converted to RPU by dividing by the strength of this promoter. The upper dashed line represents the strong P<sub>TDH3</sub> promoter and the lower dashed line is the background fluorescence of white cells. The cytometry histograms associated with these measurements are shown in Extended Data Fig. 4. The data represent the average of three experiments performed on different days. **c**, The three sensors were inserted into the genome. A representative reporter construct for the aTc-inducible system is shown (right). The repressors for each inducible system were placed under the control of a constitutive promoter (P<sub>VMA6</sub>, P<sub>FBA1</sub> or P<sub>PXR1</sub>). A natMX gene was also added for colony selection. The sequences for all of the genetic parts are provided in Supplementary Tables 5 and 8. **d**, The response functions of the three sensors are shown. Each was measured with a reporter construct integrated at the IIA.ChV locus in the genome (Supplementary Fig. 14). Only the OFF/ON values of each sensor were used as inputs to Cello 2.0. The ON values are shown as dashed red lines (100 ng ml<sup>-1</sup> aTc, 10 mM D-xylose and 20 mM IPTG). Data are shown for three experiments performed on different days. **e**, No crosstalk was observed between the three sensors. The concentrations of small molecules were: 100 ng ml<sup>-1</sup> aTc, 10 mM D-xylose and 20 mM IPTG. The data represent the average of three experiments performed on different days. Fold-induction was calculated as RPU (+inducer)/RPU (-inducer).

NOT gate response function, the input to which is the sum of the input promoters. We tested this for the nine gates where the repressor genes were encoded in the IIA.ChV locus, transcribed by P<sub>tet</sub> and P<sub>lac</sub>. Different combinations of aTc and IPTG were added and the resulting fluorescences were measured ('measured output' in Fig. 5h). This was compared with the predicted output, which was obtained when the two input promoters were summed and used with the NOT gate response function (taken from Fig. 5b). While there was some systematic error, the correlation was sufficient to use the NOT response functions to connect gates.

**Genetic circuit design automation.** Cello 2.0 maps the desired circuit to a linear DNA sequence to be inserted in a specific genetic location. For *S. cerevisiae*, we selected two genomic loci to carry the

circuit (Fig. 6a) (Supplementary Fig. 1)<sup>81</sup>. In practice, we found that maintaining the insulator order resulted in more reliable circuits. Therefore, we constrained the order of the insulators, as opposed to an order of repressor genes/gates. This is shown in Fig. 6a, where the transcription units follow the progression of 1–16, but the order of the repressor genes in the progression is random. To evaluate the difference in expression at these sites, 16 strains were built where a P<sub>tet</sub>-yfp construct was inserted at each position and the variation in expression was less than twofold, which was small enough to not disrupt gate function (Fig. 6b).

To validate design automation, a test set of three-input logic circuits were constructed (specified in Verilog, Supplementary Note 1). The sensors were defined along with their OFF/ON response (red lines in Fig. 4d) and the UCF SC1C1G1T1 was selected

(Supplementary Data 1). Cello 2.0 then parsed the Verilog text, used logic minimization to create a wiring diagram, simulated annealing to assign repressors and mapped the result to a DNA sequence according to the constraints defined in the UCF. The outputs were predicted for all combinations of inputs. The predictions were made before constructing the circuits and the DNA sequences were built exactly as specified. Six circuits were designed in this way, of which five functioned as predicted (Fig. 6c) (Methods). One circuit had one failed state, which we traced to population variability of the gate based on the CI repressor, which spans the threshold of the next gate (Extended Data Fig. 9). The growth impact of the circuits was also assessed for all of their states, of which six out of 40 demonstrated slow growth (Extended Data Fig. 10).

The dynamic responses of the five circuits were measured for >2 weeks (400 h) without selective markers (Fig. 7a). The cells were exposed to different combinations of inducers every 48 h until the circuit had transitioned through all eight states (Methods). No gross circuit failures or genetic instability were observed for any of the circuits. The circuits either had four (0x06 and 0xF6) or five layers and required much more time to reach steady state (up to 30 h) than the individual gates (~12 h). The response over time was compared with a mathematical model that was parameterized only with the empirically measured on and off times of the individual gates (Supplementary Table 2) (Methods). The model accurately captured the performance of the circuit over time, including the delays due to layering.

Transiently incorrect outputs, or glitches, can occur when the signal splits and one rapidly progresses to the end, whereas the other is delayed as it propagates through additional layers<sup>92,93</sup>. For *S. cerevisiae*, there is a long delay for the signal to propagate through a gate and this leads to prevalent glitches, which are predicted by the mathematical model. To show the relationship between the gate delays and a fault, additional experiments were performed with the 0xA1 circuit, looking at the transition from  $-/-/-$  to  $+/+/-$  (Fig. 7b). The last gate is an OR function where one input turns off faster than the other can turn on after this change in the inducers. To test this, strains were constructed that contained *rfp* reporters for the output promoters of each intermediate gate in the circuit integrated into the HO locus (Fig. 7c,d and Supplementary Table 4). Each

gate was accurately modelled using the simple ordinary differential equation (ODE), including the observed glitch.

## Discussion

Many groups have shown that you can combine regulatory interactions to build a circuit function that performs correctly at a digital level<sup>8,10,13</sup>. However, the quantitative response is not predicted. We have found that making more precise predictions requires the careful design of insulated gates and selection of where they should be carried in the cell. Philosophically, we define the UCF for a highly specified context (strain, loci and growth conditions) for which the predictions are valid. While gates may ‘work’ when inserted in a different locus, strain or media, these are not the conditions for

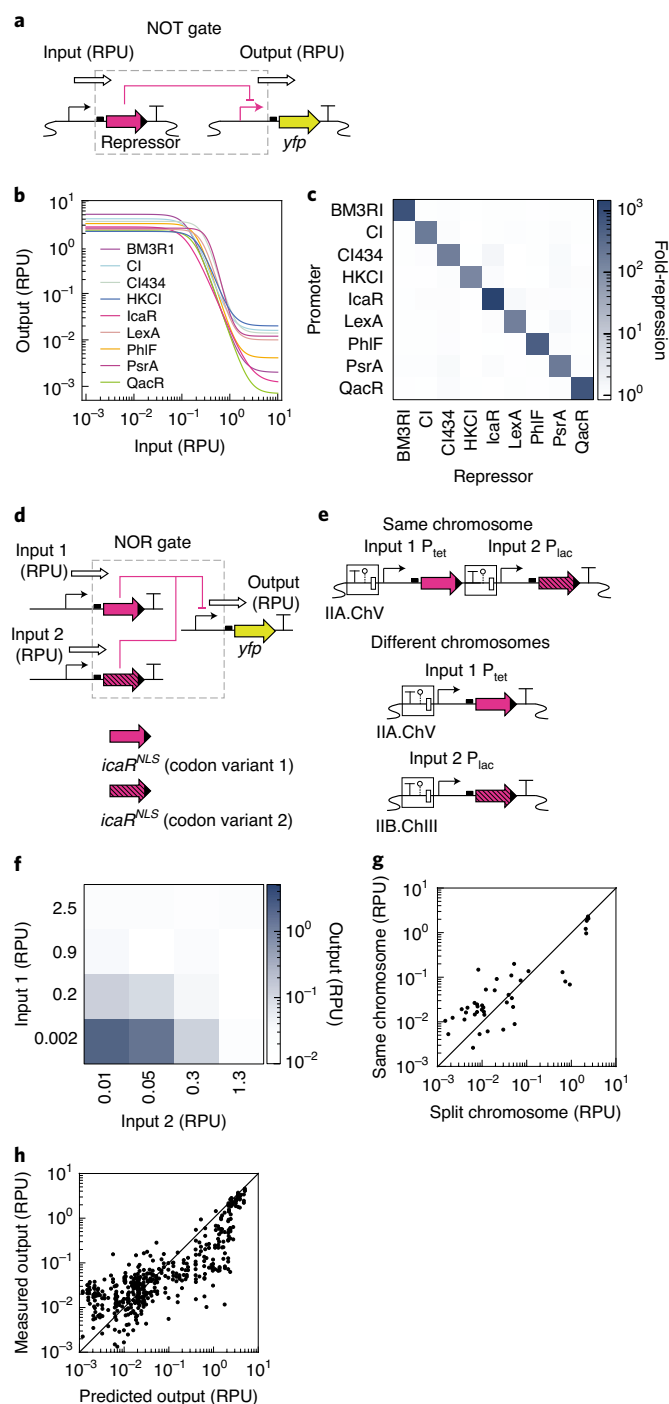


**Fig. 5 | NOT/NOR gates.** **a**, The NOT gate design is based on repressors that contain a carboxy-terminal nuclear localization signal (black). **b**, NOT gate response functions. The data for the response of each gate were fit to equation (1) (colour coded by repressor). The data used for these fits are shown in Extended Data Figs. 7 and 8. The concentrations of IPTG (from left to right) were: 0, 0.1, 0.25, 0.5, 1, 1.5, 2, 2.5, 3, 5, 10 and 20 mM. **c**, Orthogonality of the gates. The promoters and reporters were integrated into IIB.ChIII and the repressors ( $P_{tet}$  controlled) were integrated into IIA.ChV under aTc control (0 or 100 ng  $\mu\text{l}^{-1}$  aTc added). The fold-repression was calculated as RPU ( $-$ aTc)/RPU ( $+$ aTc). **d**, The design of the NOR gate is shown, where each input promoter transcribes a different copy of the repressor gene with different codon assignments. **e**, The two copies of the repressor were integrated at the same genomic locus (top) or at two loci (bottom). **f**, The response of the IcaR NOR gate at IIA.ChV is shown as a function of both inducers. IPTG was added at 0, 0.5, 2 and 20 mM (input 1) and aTc was added at 0, 20, 30 and 100 ng  $\text{ml}^{-1}$  (input 2). **g**, The IcaR NOR gate was compared when the repressor genes were on the same chromosome or split between two (as shown in **e**). **h**, Comparison of the output of a NOR gate with that predicted by using the corresponding NOT gate response function. For all nine gates, the two-dimensional response was measured (as in **f**) and compared with that predicted using the one-dimensional response function (**b**) and summing the activities of the input promoters. The data represent the average of three experiments (**c** and **f**) or individual experiments (**g** and **h**) performed on different days.

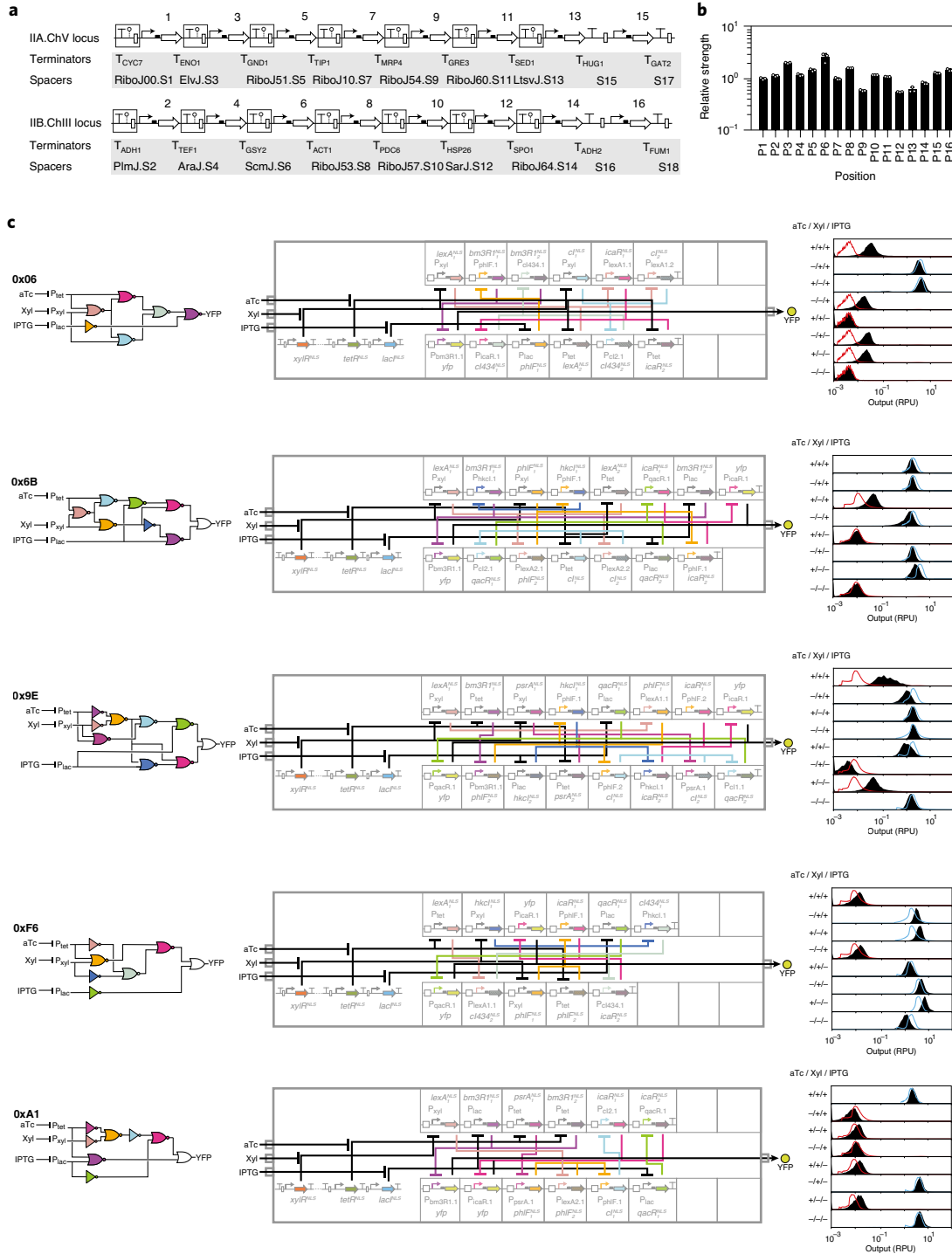


**Fig. 6 | Genetic circuits.** **a**, Each circuit occupies two chromosomal locations. The insulator order is defined and the gates were assigned to positions 1–16 until there were no more gates associated with the circuit. The remaining insulators that were not used were not included in the circuit DNA. **b**, Expression differences when an aTc-inducible promoter and yfp reporter were inserted at each position. For these measurements, the insulators before and after the position were included unless it appeared at an edge. The relative strength is the measured fluorescence (with 100 ng  $\mu$ l<sup>-1</sup> aTc), reported relative to position 1. The data represent the average of three experiments performed on different days. **c**, Circuits designed by Cello 2.0. The boxes correspond to the positions in **a** and the squares represent the insulators. Cytometry distributions are shown for the circuit output in the presence or absence of 100 ng ml<sup>-1</sup> aTc, 10 mM D-xylose and 20 mM IPTG (Methods). The solid red and blue distributions represent those predicted by Cello 2.0 when the output was low or high, respectively. For all histograms, at least three experiments were performed on different days with similar results.

which they were designed, and this may produce a subtly different quantitative response that propagates to other gates, with the potential of ultimately leading to a circuit failure. Achieving precise predictions through design automation requires that the gates be

re-characterized in the new strain or genetic location of interest and these data are then used to build a new UCF. While going through the process of building new gates and a new UCF is initially difficult, after it is complete, it simplifies the design of genetic circuits

for that host. In fact, a circuit function can be re-mapped to DNA for different hosts in seconds just by selecting a new UCF in Cello 2.0. We now have examples where the same circuit specified with Verilog code has been automatically mapped either to an *E. coli* plasmid (Eco1C2G2T2) or a yeast chromosome (SC1C1G1T1). The Verilog files that appear in this manuscript are relatively simple, but one can imagine a future where genetic designs are shared at this higher and more abstract level and then re-compiled to new organisms as needed.

Large genetic engineering projects will require regulatory networks to coordinate responses; for example, turning on metabolic valves at the right times during growth, managing energy and materials resources, dividing tasks among a population and staging processes. These networks must function precisely in different states and implement dynamic responses. As the need for more complex regulatory networks grows, they will become too large to construct in an ad hoc manner and they will have too many states to be optimized by directed evolution. Design automation will be relied on increasingly frequently to balance the constraints and put together the multitude of DNA parts required.

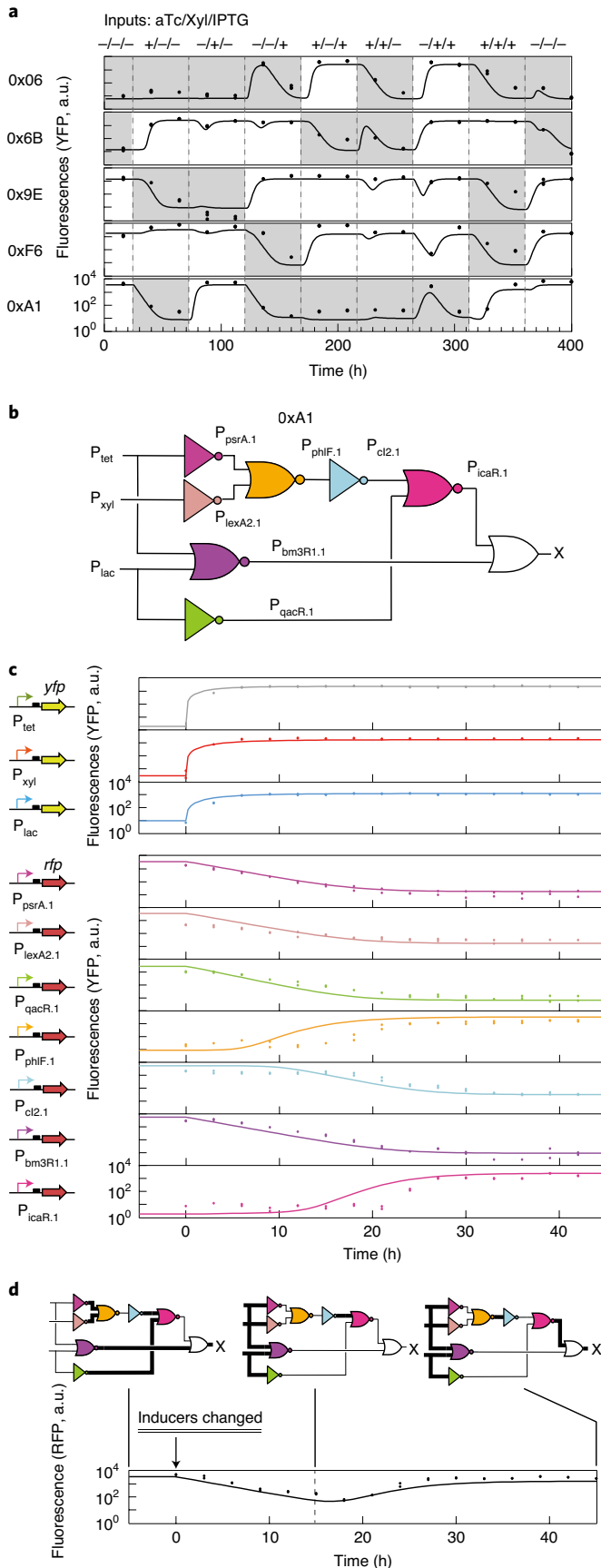
## Methods

**Strain, media and reagents.** *S. cerevisiae* BY4741 MAT $\alpha$  his3Δ1 leu2Δ0 met15Δ0 ura3Δ0, an S288C derivative, was the parent strain unless otherwise noted. *S. cerevisiae* CENPK.113-7D was used to measure the native promoter–terminator combinations. Cells were grown in either YPD broth (Sigma–Aldrich; Y1375) or synthetic drop-out medium (SD; Sunrise; 1701). SD-Ura (Sunrise; 1703), SD-Leu (Sunrise; 1707), SD-His (Sunrise; 1705) and SD-Ura-Leu (Sunrise; 1721) media to select the correct clones for genome integration or maintain plasmids with corresponding markers. When indicated, 2% galactose (Sigma–Aldrich; G0750) was added to SD without glucose (Sunrise; 1797) medium. The antibiotic 100  $\mu\text{g ml}^{-1}$  nourseothricin (Gold Biotechnology; N-500) was used for NatMX marker selection. 1.8% agar (Bacto; 214010) was used for agar plates. The inducers used were: IPTG (Sigma–Aldrich; I6758), aTc (Sigma–Aldrich; 37919), D-xylose (Xyl; Sigma–Aldrich; X1500) and vanillic acid (Sigma–Aldrich; 94770). The reporter genes used for these experiments were *yfp* and *rfp* codon optimized for yeast<sup>94–96</sup>.

**Collation of yeast part library.** Promoters and terminators were sourced from yeast part collections<sup>53,62,70,74,97–100</sup>, yeast transcriptomic data<sup>101</sup> and other yeasts in the *Saccharomyces* genus using the Broad Institute Fungal Orthogroups Repository<sup>102</sup>. Parts were mutated to eliminate BsaI and BpiI restriction enzyme sites. For parts sourced from transcriptomic data, the sequence length was adjusted to capture the region of reduced nucleosome occupancy, as defined by Segal and co-workers<sup>103</sup>, and to avoid including proximal genome features. Promoters

**Fig. 7 | Circuit dynamics.** **a**, The five circuits were cycled between states for 400 h (17 d). Cells containing the circuits were cultured as described in the Methods, diluting into fresh media daily. Every 2 d, different combinations of inducers were added to the media (shown at the top). The experimental data points are shown and compared with the dynamics predicted with the ODE (Methods). The data points represent biological triplicates, collected concurrently. **b**, The circuit diagram of 0xA1 is shown, including the promoters corresponding to each wire. **c**, Cells containing the circuit were grown with the  $-/-/-$  combination of inducers until steady state and then transferred into fresh media with the  $+/+/-$  combination of inducers. The responses of each of the sensors and gates to this transition are shown. The sensors were measured using strains that only contained their output promoter fused to *yfp* (no circuit) (*S. cerevisiae* CY637int, CY639int or CY928int) (Supplementary Table 4). The other wires were analysed by fusing the promoter shown in **b** to *rfp* and integrating the reporter into the chromosome IV, 48031...46271, HO locus. The points show experimental duplicates collected over different days. The lines show the predictions from the ODE model. **d**, The output of the circuit (X) is shown for the  $-/-/-$  to  $+/+/-$  transition, highlighting a fault. The circuit diagrams show the wires with active RNAP flux at the different time points. The middle diagram shows the delay leading to the fault when one of the inputs to the last NOR gate was turned off before the other could turn on. The data represent two experiments performed on different days.

and terminators were synthesized using GeneArt, or from the US Department of Energy Joint Genome Institute, or amplified from *S. cerevisiae* genomic DNA or yeast shuttle vectors. The sequences of all genetic parts are provided in Supplementary Tables 7 and 8.



**Cell culture conditions for the characterization of parts, gates and circuits.** The following protocol was used for all promoter, terminator and insulator experiments except those noted in the next section. Frozen stocks were streaked and grown overnight. A single colony was picked into 500 µl SD medium (with auxotrophic selection) and inducers (if required) in a 2-ml 96-deep-well plate (Plate One; 1896-2000) sealed with AeraSeal film (Excel Scientific; BS25). The plates were incubated at 30 °C and 900 r.p.m. in a Multitron shaker incubator for 24 h. For circuits containing two or more layers, this culture was diluted 200-fold a second time and grown again under the same conditions for an additional 24 h. Then, the overnight culture was diluted to OD<sub>600</sub> = 0.005 (Synergy H1 plate reader; BioTek) by adding 2.5 µl culture to 497.5 µl fresh SD medium (without selection, but with inducers if required) in a 2-ml 96-deep-well plate and sealed with AeraSeal film. The cultures are grown at 30 °C and 900 r.p.m. in a Multitron shaker incubator for 16 h. After growth, a 20 µl culture was added to 180 µl phosphate-buffered saline (PBS; Omnipur; 6505-OP) with 10 µg ml<sup>-1</sup> cycloheximide (Sigma-Aldrich; 227048) into a 96-well U-bottomed plate (Corning; 3367) and incubated for 1 h at room temperature for cytometry analysis. In addition, 200 µl of this culture was transferred into 96-well black-walled optical-bottomed plates (Nunc; 165305) to measure the cell density.

**Characterization of promoter–terminator pairs.** The following protocol was used for promoter–terminator pair characterization in Fig. 3a. Note that the host strain of this experiment was *S. cerevisiae* CENPK.113-7D, which is different from the one used for the remainder of the work in this manuscript. The expression strengths of promoter and terminator pairs were determined using Venus YFP<sup>96</sup> and the constructs are shown in Supplementary Fig. 16. Note that this reporter gene is different from the one used for the remainder of the work in this manuscript. A single colony of yeast transformants was picked into 500 µl SD medium (with nourseothricin selection and 2% glucose or 2% galactose as the carbon source) into a 2-ml 96-deep-well plate (Plate One; 1896-2000) sealed with AeraSeal film (Excel Scientific; BS25). The plates were incubated at 30 °C and 900 r.p.m. in a Multitron shaker incubator for 48 h. Then, the culture was diluted by adding 10 µl culture into 490 µl fresh SD medium (with nourseothricin selection and 2% glucose or 2% galactose as the carbon source) in a 2-ml 96-deep-well plate and sealed with AeraSeal film. The cultures were grown at 30 °C and 900 r.p.m. in a Multitron shaker incubator for 24 h. After growth, 20 µl of the culture was added to 180 µl PBS (Omnipur; 6505-OP) with 10 µg ml<sup>-1</sup> cycloheximide (Sigma-Aldrich, 227048) into a 96-well U-bottomed plate (Corning; 3367) and incubated for 1 h at room temperature for cytometry analysis.

**Flow cytometry.** Fluorescences were measured for >20,000 events for each sample with an LSRII Fortessa flow cytometer with HTS (BD Biosciences). FITC-A and PE Texas-A channels were chosen for YFP and RFP measurement, respectively. Data were processed using FlowJo (TreeStar) to obtain the median of fluorescence, gated by the width of the forward scatter and the side scatter (FSC-W/SSC-W)<sup>23</sup>. The fold-repression was calculated by (YFP<sub>unrepressed</sub> - YFP<sub>0</sub>)/(YFP<sub>repressed</sub> - YFP<sub>0</sub>). The fold-induction was calculated by (YFP<sub>induced</sub> - YFP<sub>0</sub>)/(YFP<sub>uninduced</sub> - YFP<sub>0</sub>). YFP<sub>unrepressed</sub> and YFP<sub>repressed</sub> were the fluorescence of the ON and OFF states of the NOT gate strain (YFP as reporter). YFP<sub>induced</sub> and YFP<sub>uninduced</sub> were the fluorescence of the sensor strain with (100 ng ml<sup>-1</sup> aTc, 10 mM xylose and 20 mM IPTG, respectively) and without inducer. YFP<sub>0</sub> was that from white cells (*S. cerevisiae* BY4741).

**Calculation of RPU.** To characterize a promoter, the median fluorescence values (YFP) were measured along with the fluorescence of the RPU reference strain (*S. cerevisiae* CY671int) (YFP<sub>RPU</sub>) and that from white cells (*S. cerevisiae* BY4741) (YFP<sub>0</sub>), all under the same growth conditions as described above. The promoter activity in RPU was calculated by RPU = (YFP - YFP<sub>0</sub>)/(YFP<sub>RPU</sub> - YFP<sub>0</sub>).

**Measurement of growth rates.** Cell density was measured as the OD<sub>600</sub> using a Synergy H1 plate reader (BioTek). We also measured background OD<sub>600</sub> using a 200-µl aliquot of media without cells, which was subtracted from the OD<sub>600</sub> value for a sample. When presented as normalized, the measured value was divided by that measured for the same strain without inducers.

**Measurement of gate and sensor dynamics.** Colonies were picked into 500 µl SD medium (with auxotrophic selection) with inducers (initial states, if required) in a 2-ml 96-deep-well plate (Plate One; 1896-2000) sealed with AeraSeal film (Excel Scientific; BS25). The plates were incubated at 30 °C and 900 r.p.m. in a Multitron shaker incubator for 24 h. Then, the overnight culture was diluted to OD<sub>600</sub> = 0.005 (Synergy H1 plate reader; BioTek) by adding 2.5 µl culture to 497.5 µl fresh SD medium (without auxotrophic selection, but with inducers if required) in a 2-ml 96-deep-well plate and sealed with AeraSeal film. The cultures were grown at 30 °C and 900 r.p.m. in a Multitron shaker incubator for 16 h. Then, 500 µl of the culture collected at OD<sub>600</sub> = 1.0 was spun down by centrifugation at 4 °C and 500 g for 5 min. After removing the supernatants, the cell pellet was resuspended in 500 µl fresh SD-glucose media (with final state inducers) and then diluted 1:20 into 500 µl fresh SD-glucose media (with final state inducers) at OD<sub>600</sub> = 0.05 (Synergy H1 plate reader; BioTek) in a 2-ml 96-deep-well plate sealed with

AeraSeal film. The plates were incubated at 30 °C and 900 r.p.m. in a Multitron shaker incubator. Aliquots (20 µl) of the culture were collected every 3 h for flow cytometry measurement. During the measurement, the culture was 1:10 diluted to OD<sub>600</sub> = 0.05 in 500 µl fresh SD-glucose media (with inducers if required) every 12 h.

**Model of gate dynamics.** The model followed the approach described previously and the detailed derivation and fitting procedure are presented in that manuscript<sup>28</sup>. Briefly, the model has two parameters that capture how quickly a gate moved to its steady-state output given the state of the input. For example, if the input was ON and the gate output *y* was OFF, then if the input changed to being OFF, the gate output was lower than its steady-state value *y<sub>ss</sub>* and it would turn on at a rate dictated by the parameter  $\tau_{ON}$ . In the opposite case, when the input was OFF and then turned ON, *y* would be higher than *y<sub>ss</sub>* and would have to turn off, which it would do at a rate following the parameter  $\tau_{OFF}$ . This response was captured by the following differential equation describing a single gate:

$$\frac{dy}{dt} = \begin{cases} \tau_y^{ON}(y_{ss} - y) & \text{if } y < y_{ss} \\ \tau_y^{OFF}(y_{ss} - y) & \text{otherwise} \end{cases} \quad (2)$$

where the relationship between *y<sub>ss</sub>* and the input *x* is provided by equation (1). Note that dy/dt describes the rate of change of the RNAP flux from the promoter and not the reporter expression and maturation, which is mathematically separated. We developed a fitting procedure to extract the parameters  $\tau_{ON}$  and  $\tau_{OFF}$  using the empirical measurements described in the previous section. First, the dynamic response of the sensor was measured (Extended Data Fig. 5), from which we extracted the response time of the sensor's output promoter upon addition or removal of the inducer and the rate associated with the expression and folding of the reporter protein. YFP degradation was assumed to be dominated by the cell doubling time. To fit the data for each sensor, the following equations were used:

$$\frac{dx}{dt} = \tau_x(x_{ss} - x) \quad \text{and} \quad (3)$$

$$\frac{d[YFP]}{dt} = \tau_{ON}^{YFP}x - \tau_{OFF}^{YFP}[YFP], \quad (4)$$

where *x* is the RNAP flux from the sensor's output promoter reported in RPU. The results from this process were  $\tau_{ON}/\tau_{OFF}$  values of the IPTG, aTc and D-xylose sensor of 0.2/0.25, 0.3/0.3 and 0.3/0.3. The YFP response was  $\tau_{ON}^{YFP} = 944 \text{ au} \times \text{RPU}^{-1} \text{ h}^{-1}$  and  $\tau_{OFF}^{YFP} = 2.3 \text{ h}^{-1}$ . Then, the on and off dynamics of each gate were measured. To fit the data for each gate, the following equations were used:

$$\frac{dx}{dt} = \tau_x(x_{ss} - x) \quad (5)$$

$$\frac{dy}{dt} = \tau_y(y_{ss} - y) \quad (6)$$

$$\frac{d[YFP]}{dt} = \tau_{ON}^{YFP}y - \tau_{OFF}^{YFP}[YFP] \quad (7)$$

The results of the fitting procedure are shown in Extended Data Figs. 7 and 8 and the parameters for each gate are shown in Supplementary Table 2.

**New capabilities and features of Cell 2.0.** Cello 2.0 encompasses a suite of features to expand circuit design to new species. This requires flexibility in how gates are defined, how organizational rules are written to map the gates to a DNA sequence, and where the circuit DNA is carried. Collectively, this enables Cello to map a Verilog design to multiple species with minimal user intervention. In addition, Cello 2.0 has been designed to be compatible with the greater Synthetic Biology software development community through compatibility with SynBioHub and SBOL data standards<sup>104,105</sup>, with the former linking the Cello designs to a process workflow for construction and testing. The graphic user interface has also been modified so that a user can set up a project and store sensor collections and there is improved error reporting. Cello has been modified to use the logic synthesis tool Yosys, which implements the Verilog 2005 specification nearly in its entirety (Institute of Electrical and Electronics Engineers standard 1364-2005) so that the circuit design can be exchanged between different software tools and domains. This extended language support is required for the specification of large circuits, distributing circuits across multiple cells, and for the design of sequential logic.

**UCF format tailored for diverse organisms.** Each UCF is a JSON file that can be selected using the Cello graphic user interface in the Library tab of a new project. To date, five UCFs are included: Eco1C1G1T1 (*E. coli* DH10b; p15a plasmid), Eco2C1G3T1 (*E. coli* DH10b; p15a plasmid; improved gates), Eco1C2G2T2 (*E. coli* DH10b; genome landing pads), Bth1C1G1T1 (*Bacteroides thetaiotaomicron*; CRISPRi gates in genome) and SC1C1G1T1 (*S. cerevisiae* BY4747; in chromosome;

this work). The user first creates a new project then selects from these UCFs or uploads a new one for their own species.

**Gate architecture specification.** Cello 1.0 was hardwired for NOR gates with two input promoters in series. The new UCF structure has a JSON gate\_structure object type, which allows a user to define a gate architecture based on a collection of part types. This is critical for the *S. cerevisiae* gate architecture since: (1) two input promoters each drive a copy of the repressor gene with different DNA sequences; (2) the terminator is not part of the gate architecture; and (3) there are yeast-specific translation parts and insulators. Expanding beyond the yeast gates, this approach can be applied to other modes of regulation (for example, CRISPRi and invertases), any Boolean gate as well as more than two input promoters.

**Gate model flexibility.** Previously, the response functions were defined to have a single mathematical form and associated fit parameters. However, different gate architectures and different classes of regulators require alternative models. To accommodate this, we created a new JSON object type gate\_model that has two fields: function and parameters. The function identifier refers to a function object (for example, for *S. cerevisiae*, it is Hill\_function, defined as  $[y_{\min} + (y_{\max} - y_{\min}) \times (K^a)/(K^a + X^a)]$ ), as well as each parameter {'name': 'y<sub>min</sub>', 'map': '#!/model/parameters/y<sub>min</sub>'}, where 'map' is a pointer to a numerical value. Variables are also defined {'name': 'x', 'map': '#!/model/functions/input\_composition'}, where 'map' points to a function that, in the simplest case, sums the RPU activity of both gate inputs, as for *S. cerevisiae*.

**Expansion of rule sets for DNA mapping.** Cello uses rules, defined in the UCF, to map the circuit design to a linear DNA sequence (for example, the order and orientation of repressor genes on a plasmid). These rules were expanded to encompass the need for gate designs in new species and for their encoding in the genome. A new object type, genetic\_locations, defines the host genome, either by a link to a sequence in National Center for Biotechnology Information or by completely embedding the host genome sequence in the UCF, as well as the insert locations that can be referenced symbolically in the Eugene rule sets. Each genetic locus available for circuit inserts is assigned a symbol (for example, L1, L2 and so on). For *S. cerevisiae*, the gates can occur in 16 positions in two chromosomal locations. Rules in the UCF constrain not only the chromosomal location of each gate but also the relative positions of gates within a locus. The *S. cerevisiae* gates are separated by defined scars that are used to control gate placement; for example, in the rule 'P1\_CI434\_b AFTER KscAR AND P1\_CI434\_b BEFORE Oscar'. The *S. cerevisiae* NOR gates comprise two expression cassettes based on two copies of the repressor. The expression cassettes are intended to be separated into two different locations in the genome. For every gate, there is a rule such as OR{ AND{ 'GateX\_a BEFORE L2', 'GateX\_b AFTER L2' }, OR{ 'GateX\_a AFTER L', 'GateX\_b BEFORE L' } }, indicating that an expression cassette can be in either location, as long as it is not the location of the gate's other cassette. The parsing of these rules was also modified to make it easier for a user to compose a rule set that is interpretable by Cello.

**UCF.** The *S. cerevisiae* UCF (SC1C1G1T1) is provided in the Supplementary Data 1. The UCF contains the gate technology and associated data (response functions, including cytometry distributions, and OD<sub>600</sub> measurements). It also defines the strain, the genetic location of the circuit and the growth conditions for which the circuit design is valid. SC1C1G1T1 is based on *S. cerevisiae* strain BY4741 and the location of the circuits is *ura3*: (IIA.ChV) and *leu2*: (IIB.ChIII) (Fig. 1). For each gate, the repressor has two versions of sequences in different codons to minimize potential homologue sequences, and the targeting promoter also has a mutated version for the same reason. Eugene<sup>106</sup> rules are also included to specify the organization of gates onto a linear DNA sequence. This UCF uses the following layout rules for gates and type IIS cloning scars. Multiple gates that use the same repressor and different targeting promoters are prohibited from appearing in the same circuit. Cloning scars appear in the order A, B, C, D, E, F, G, H, I (IIA.ChV) and J, K, L, M, N, P, Q, R, S (IIB.ChIII) (Supplementary Figs. 14 and 17).

**Computational circuit design.** The Cello 2.0 software was used to design the circuit DNA sequences (note that the UCF will not work with Cello 1.0). The toxicity cut-off is 0.7 for gates and 0.5 for the complete circuit. Each circuit was specified as a Verilog text file (Supplementary Note 1). All circuits were specified as truth tables and Cello 2.0 identified the wiring diagram using logic minimization. The SC1C1G1T1 UCF was used for the calculations and is provided as Supplementary Data 1. Data for the sensors are also provided (Supplementary Table 1). The output of Cello 2.0 includes DNA sequences for the circuit, which were constructed as specified, and predictions for cytometry fluorescence data and the impact on growth.

**Circuit long-term growth and induction experiments.** Colonies were picked into 500 µl SD medium (with auxotrophic selection) and inducers (initial states, if required) in 2-ml 96-deep-well plates (Plate One; 1896-2000) sealed with AeraSeal film (Excel Scientific; BS25). The plates were incubated at 30 °C and 900 r.p.m. in a Multitron shaker incubator for 24 h. For circuits containing two or more layers, this culture was diluted 200-fold a second time and grown again under the same conditions for an additional 24 h. Then, the overnight culture

was diluted to OD<sub>600</sub>=0.005 (Synergy H1 plate reader; BioTek) by adding 2.5 µl of culture into 497.5 µl fresh SD medium (without selection, but with initial state inducers if required) in a 2-ml 96-deep-well plate and sealed with AeraSeal film. The cultures were grown at 30 °C and 900 r.p.m. in a Multitron shaker incubator for 16 h. Aliquots of 500 µl of the culture at OD<sub>600</sub>=1.0 were taken and spun down by centrifugation at 4 °C and 500g for 5 min. After removing the supernatants, the cell pellet was resuspended in 500 µl fresh SD-glucose media (with final state inducers) and then 1:20 diluted to 500 µl fresh SD-glucose media (with final state inducers) at OD<sub>600</sub>=0.05 (Synergy H1 plate reader; BioTek) in 2-ml 96-deep-well plates sealed with AeraSeal film. The plates were incubated at 30 °C and 900 r.p.m. in a Multitron shaker incubator. The same dilution process (without the spin-down step) was repeated every 12 h for continuous exponential growth. The cells were collected every 3 h for flow cytometer measurement. For the dynamic experiments performed over 400 h, cells were resuspended and diluted to OD<sub>600</sub>=0.005 (Synergy H1 plate reader; BioTek) in fresh SD-glucose media with inducers every 24 h. The fluorescence was measured by flow cytometry at 16 h after dilution.

**Simulation of circuit dynamics.** The RPU outputs for all gates under initial conditions were first obtained from Cello 2.0. Then, we performed a numerical analysis from time 0 using the ODEs for the circuit. For example, the equations for the 0x06 circuit are shown below:

For sensors

$$\frac{dx_{tetR}}{dt} = \begin{cases} \tau_{tetR}^{ON}(x_{tetR,ss} - x_{tetR}) & \text{if } x_{tetR} < x_{tetR,ss} \\ \tau_{tetR}^{OFF}(x_{tetR,ss} - x_{tetR}) & \text{otherwise} \end{cases}$$

$$\frac{dx_{xyLR}}{dt} = \begin{cases} \tau_{xyLR}^{ON}(x_{xyLR,ss} - x_{xyLR}) & \text{if } x_{xyLR} < x_{xyLR,ss} \\ \tau_{xyLR}^{OFF}(x_{xyLR,ss} - x_{xyLR}) & \text{otherwise} \end{cases}$$

$$\frac{dx_{lacI}}{dt} = \begin{cases} \tau_{lacI}^{ON}(x_{lacI,ss} - x_{lacI}) & \text{if } x_{lacI} < x_{lacI,ss} \\ \tau_{lacI}^{OFF}(x_{lacI,ss} - x_{lacI}) & \text{otherwise} \end{cases}$$

For gates

$$\frac{dy_{icaR}}{dt} = \begin{cases} \tau_{icaR}^{ON}\left(y_{icaR,min} + (y_{icaR,max} - y_{icaR,min}) \frac{K_{icaR}^{n_{icaR}}}{K_{icaR}^{n_{icaR}} + f(x_{tetR}, x_{lexA})^{n_{icaR}}} - y_{icaR}\right) \\ \quad \text{if } y_{icaR} < y_{icaR,ss} \\ \tau_{icaR}^{OFF}\left(y_{icaR,min} + (y_{icaR,max} - y_{icaR,min}) \frac{K_{icaR}^{n_{icaR}}}{K_{icaR}^{n_{icaR}} + f(x_{tetR}, x_{lexA})^{n_{icaR}}} - y_{icaR}\right) \\ \quad \text{otherwise} \end{cases}$$

$$\frac{dy_{lexA}}{dt} = \begin{cases} \tau_{lexA}^{ON}\left(y_{lexA,min} + (y_{lexA,max} - y_{lexA,min}) \frac{K_{lexA}^{n_{lexA}}}{K_{lexA}^{n_{lexA}} + f(x_{tetR}, x_{xyLR})^{n_{lexA}}} - y_{lexA}\right) \\ \quad \text{if } y_{lexA} < y_{lexA,ss} \\ \tau_{lexA}^{OFF}\left(y_{lexA,min} + (y_{lexA,max} - y_{lexA,min}) \frac{K_{lexA}^{n_{lexA}}}{K_{lexA}^{n_{lexA}} + f(x_{tetR}, x_{xyLR})^{n_{lexA}}} - y_{lexA}\right) \\ \quad \text{otherwise} \end{cases}$$

$$\frac{dy_{phlF}}{dt} = \begin{cases} \tau_{phlF}^{ON}\left(y_{phlF,min} + (y_{phlF,max} - y_{phlF,min}) \frac{K_{phlF}^{n_{phlF}}}{K_{phlF}^{n_{phlF}} + x_{lacI}^{n_{phlF}}} - y_{phlF}\right) \\ \quad \text{if } y_{phlF} < y_{phlF,ss} \\ \tau_{phlF}^{OFF}\left(y_{phlF,min} + (y_{phlF,max} - y_{phlF,min}) \frac{K_{phlF}^{n_{phlF}}}{K_{phlF}^{n_{phlF}} + x_{lacI}^{n_{phlF}}} - y_{phlF}\right) \\ \quad \text{otherwise} \end{cases}$$

$$\frac{dy_{cl}}{dt} = \begin{cases} \tau_{cl}^{ON}\left(y_{cl,min} + (y_{cl,max} - y_{cl,min}) \frac{K_{cl}^{n_{cl}}}{K_{cl}^{n_{cl}} + f(y_{lexA}, x_{xyLR})^{n_{cl}}} - y_{cl}\right) \\ \quad \text{if } y_{cl} < y_{cl,ss} \\ \tau_{cl}^{OFF}\left(y_{cl,min} + (y_{cl,max} - y_{cl,min}) \frac{K_{cl}^{n_{cl}}}{K_{cl}^{n_{cl}} + f(y_{lexA}, x_{xyLR})^{n_{cl}}} - y_{cl}\right) \\ \quad \text{otherwise} \end{cases}$$

$$\frac{dy_{cl434}}{dt} = \begin{cases} \tau_{cl434}^{ON}\left(y_{cl434,min} + (y_{cl434,max} - y_{cl434,min}) \frac{K_{cl434}^{n_{cl434}}}{K_{cl434}^{n_{cl434}} + f(y_{cl}, x_{icar})^{n_{cl434}}} - y_{cl434}\right) \\ \quad \text{if } y_{cl434} < y_{cl434,ss} \\ \tau_{cl434}^{OFF}\left(y_{cl434,min} + (y_{cl434,max} - y_{cl434,min}) \frac{K_{cl434}^{n_{cl434}}}{K_{cl434}^{n_{cl434}} + f(y_{cl}, x_{icar})^{n_{cl434}}} - y_{cl434}\right) \\ \quad \text{otherwise} \end{cases}$$

$$\frac{dy_{bm3R1}}{dt} = \begin{cases} \tau_{bm3R1}^{ON}\left(y_{bm3R1,min} + (y_{bm3R1,max} - y_{bm3R1,min}) \frac{K_{bm3R1}^{n_{bm3R1}}}{K_{bm3R1}^{n_{bm3R1}} + f(y_{cl}, y_{cl434})^{n_{bm3R1}}} - y_{bm3R1}\right) \\ \quad \times \frac{K_{bm3R1}^{n_{bm3R1}}}{K_{bm3R1}^{n_{bm3R1}} + f(y_{cl}, y_{cl434})^{n_{bm3R1}}} - y_{bm3R1} \quad \text{if } y_{bm3R1} < y_{bm3R1,ss} \\ \tau_{bm3R1}^{OFF}\left(y_{bm3R1,min} + (y_{bm3R1,max} - y_{bm3R1,min}) \frac{K_{bm3R1}^{n_{bm3R1}}}{K_{bm3R1}^{n_{bm3R1}} + f(y_{cl}, y_{cl434})^{n_{bm3R1}}} - y_{bm3R1}\right) \\ \quad \times \frac{K_{bm3R1}^{n_{bm3R1}}}{K_{bm3R1}^{n_{bm3R1}} + f(y_{cl}, y_{cl434})^{n_{bm3R1}}} - y_{bm3R1} \quad \text{otherwise} \end{cases}$$

$$\frac{dYFP}{dt} = \tau_{ON}^{YFP} y_{bm3R1} - \tau_{OFF}^{YFP} YFP,$$

(8)

where  $y_i/x_i$  is the output for gate/sensor  $i$  and  $y_{i,ss}/x_{i,ss}$  is the steady-state output (both in RPU). The term  $f(y_i, y_j) = y_i + y_j$  captures the input into each gate, in this case a simple sum of the input promoter activities. The equations were solved by MATLAB scripts, using the ODE solver ODE15s. All scripts are available on GitHub (<https://github.com/VoigtLab>).

**Reporting Summary.** Further information on research design is available in the Nature Research Reporting Summary linked to this article.

## Data availability

Genetic part sequences and the UCF file SC1C1G1T1.UCF are available in Supplementary Data 1. The data that support the findings of this study are available from the corresponding author upon reasonable request. Plasmids and cloning strains generated in this study will be available from Addgene ([https://www.addgene.org/Christopher\\_Voigt/](https://www.addgene.org/Christopher_Voigt/)) and the corresponding author upon request. Source data are provided with this paper.

## Code availability

The Cello 2.0 software and code are freely available at <http://www.cellocad.org/> and <https://github.com/CIDARLAB/Cello-v2>.

Received: 20 January 2020; Accepted: 17 June 2020;

Published online: 03 August 2020

## References

- Ellis, T., Wang, X. & Collins, J. J. Diversity-based, model-guided construction of synthetic gene networks with predicted functions. *Nat. Biotechnol.* **27**, 465–471 (2009).
- Krivoruchko, A., Siewers, V. & Nielsen, J. Opportunities for yeast metabolic engineering: lessons from synthetic biology. *Biotechnol. J.* **6**, 262–276 (2011).
- Billingsley, J. M., DeNicola, A. B. & Tang, Y. Technology development for natural product biosynthesis in *Saccharomyces cerevisiae*. *Curr. Opin. Biotechnol.* **42**, 74–83 (2016).
- Geva, P. et al. Increased copper bioremediation ability of new transgenic and adapted *Saccharomyces cerevisiae* strains. *Environ. Sci. Pollut. Res. Int.* **23**, 19613–19625 (2016).
- Qian, S. & Cirino, P. C. Using metabolite-responsive gene regulators to improve microbial biosynthesis. *Curr. Opin. Chem. Eng.* **14**, 93–102 (2016).
- Ferreira, R. et al. Model-assisted fine-tuning of central carbon metabolism in yeast through dCas9-based regulation. *ACS Synth. Biol.* **8**, 2457–2463 (2019).
- Ajo-Franklin, C. M. et al. Rational design of memory in eukaryotic cells. *Genes Dev.* **21**, 2271–2276 (2007).
- Marucci, L. et al. How to turn a genetic circuit into a synthetic tunable oscillator, or a bistable switch. *PLoS ONE* **4**, e8083 (2009).
- Buchler, N. E. & Cross, F. R. Protein sequestration generates a flexible ultrasensitive response in a genetic network. *Mol. Syst. Biol.* **5**, 272 (2009).
- Regot, S. et al. Distributed biological computation with multicellular engineered networks. *Nature* **469**, 207–211 (2011).
- Blount, B. A., Weenink, T. & Ellis, T. Construction of synthetic regulatory networks in yeast. *FEBS Lett.* **586**, 2112–2121 (2012).
- Yamanishi, M. & Matsuyama, T. A modified Cre-lox genetic switch to dynamically control metabolic flow in *Saccharomyces cerevisiae*. *ACS Synth. Biol.* **1**, 172–180 (2012).
- Youk, H. & Lim, W. A. Secreting and sensing the same molecule allows cells to achieve versatile social behaviors. *Science* **343**, 1242782 (2014).
- Ryu, J. & Park, S.-H. Simple synthetic protein scaffolds can create adjustable artificial MAPK circuits in yeast and mammalian cells. *Sci. Signal.* **8**, ra66 (2015).
- Khakhar, A. et al. Cell-cell communication in yeast using auxin biosynthesis and auxin responsive CRISPR transcription factors. *ACS Synth. Biol.* **5**, 279–286 (2015).
- Rantasalo, A. et al. Synthetic transcription amplifier system for orthogonal control of gene expression in *Saccharomyces cerevisiae*. *PLoS ONE* **11**, e0148320 (2016).
- Aranda-Diaz, A. et al. Robust synthetic circuits for two-dimensional control of gene expression in yeast. *ACS Synth. Biol.* **6**, 545–554 (2017).
- Ryo, S. et al. Positive feedback genetic circuit incorporating a constitutively active mutant Gal3 into yeast GAL induction system. *ACS Synth. Biol.* **6**, 928–935 (2017).
- Chen, B. et al. Synthetic biology toolkits and applications in *Saccharomyces cerevisiae*. *Biotechnol. Adv.* **36**, 1870–1881 (2018).
- Yang, Y., Nemhauser, J. L. & Klavins, E. Synthetic bistability and differentiation in yeast. *ACS Synth. Biol.* **8**, 929–936 (2019).
- Ng, A. H. et al. Modular and tunable biological feedback control using a de novo protein switch. *Nature* **572**, 265–269 (2019).
- Langan, R. A. et al. De novo design of bioactive protein switches. *Nature* **572**, 205–210 (2019).
- Ottoz, D. S., Rudolf, F. & Stelling, J. Inducible, tightly regulated and growth condition-independent transcription factor in *Saccharomyces cerevisiae*. *Nucleic Acids Res.* **42**, e130 (2014).
- Gander, M. W. et al. Digital logic circuits in yeast with CRISPR-dCas9 NOR gates. *Nat. Commun.* **8**, 15459 (2017).
- Zong, Y. et al. Insulated transcriptional elements enable precise design of genetic circuits. *Nat. Commun.* **8**, 52 (2017).
- Bashor, C. J. et al. Complex signal processing in synthetic gene circuits using cooperative regulatory assemblies. *Science* **364**, 593–597 (2019).
- Nielsen, A. A. et al. Genetic circuit design automation. *Science* **352**, aac7341 (2016).
- Shin, J. et al. Programming *Escherichia coli* to function as a digital display. *Mol. Syst. Biol.* **16**, e9401 (2020).
- Taketani, M. et al. Genetic circuit design automation for the gut resident species *Bacteroides thetaiotaomicron*. *Nat. Biotechnol.* <https://doi.org/10.1038/s41587-020-0468-5> (2020).
- Tamsir, A., Tabor, J. J. & Voigt, C. A. Robust multicellular computing using genetically encoded NOR gates and chemical ‘wires’. *Nature* **469**, 212–215 (2011).
- Nielsen, A. A. & Voigt, C. A. Multi-input CRISPR/Cas genetic circuits that interface host regulatory networks. *Mol. Syst. Biol.* **10**, 763 (2014).
- Canton, B., Labno, A. & Endy, D. Refinement and standardization of synthetic biological parts and devices. *Nat. Biotechnol.* **26**, 787–793 (2008).
- Kelly, J. R. et al. Measuring the activity of BioBrick promoters using an in vivo reference standard. *J. Biol. Eng.* **3**, 4 (2009).
- Davis, J. H., Rubin, A. J. & Sauer, R. T. Design, construction and characterization of a set of insulated bacterial promoters. *Nucleic Acids Res.* **39**, 1131–1141 (2011).
- Lou, C. et al. Ribozyme-based insulator parts buffer synthetic circuits from genetic context. *Nat. Biotechnol.* **30**, 1137–1142 (2012).
- Chen, Y. J. et al. Characterization of 582 natural and synthetic terminators and quantification of their design constraints. *Nat. Methods* **10**, 659–664 (2013).
- Nielsen, A. A., Segall-Shapiro, T. H. & Voigt, C. A. Advances in genetic circuit design: novel biochemistries, deep part mining, and precision gene expression. *Curr. Opin. Chem. Biol.* **17**, 878–892 (2013).
- Carr, S. B., Beal, J. & Densmore, D. M. Reducing DNA context dependence in bacterial promoters. *PLoS ONE* **12**, e0176013 (2017).
- Brown, C. R. & Silver, P. A. Transcriptional regulation at the nuclear pore complex. *Curr. Opin. Genet. Dev.* **17**, 100–106 (2007).
- Deniz, O. et al. Physical properties of naked DNA influence nucleosome positioning and correlate with transcription start and termination sites in yeast. *BMC Genomics* **12**, 489 (2011).
- Jansen, A. et al. Distal chromatin structure influences local nucleosome positions and gene expression. *Nucleic Acids Res.* **40**, 3870–3885 (2012).
- Curran, K. A. et al. Design of synthetic yeast promoters via tuning of nucleosome architecture. *Nat. Commun.* **5**, 4002 (2014).
- Ptak, C., Aitchison, J. D. & Wozniak, R. W. The multifunctional nuclear pore complex: a platform for controlling gene expression. *Curr. Opin. Cell Biol.* **28**, 46–53 (2014).
- Nguyen, H. Q. & Bosco, G. Gene positioning effects on expression in eukaryotes. *Annu. Rev. Genet.* **49**, 627–646 (2015).
- Porrúa, O. & Libri, D. Transcription termination and the control of the transcriptome: why, where and how to stop. *Nat. Rev. Mol. Cell Biol.* **16**, 190–202 (2015).
- Uwimana, N. et al. Bidirectional terminators in *Saccharomyces cerevisiae* prevent cryptic transcription from invading neighboring genes. *Nucleic Acids Res.* **45**, 6417–6426 (2017).
- Riethoven, J. J. Regulatory regions in DNA: promoters, enhancers, silencers, and insulators. *Methods Mol. Biol.* **674**, 33–42 (2010).
- Gaszner, M. & Felsenfeld, G. Insulators: exploiting transcriptional and epigenetic mechanisms. *Nat. Rev. Genet.* **7**, 703–713 (2006).
- Scott, K. C., Merrett, S. L. & Willard, H. F. A heterochromatin barrier partitions the fission yeast centromere into discrete chromatin domains. *Curr. Biol.* **16**, 119–129 (2006).
- West, A. G., Gaszner, M. & Felsenfeld, G. Insulators: many functions, many mechanisms. *Genes Dev.* **16**, 271–288 (2002).
- Juven-Gershon, T. & Kadonaga, J. T. Regulation of gene expression via the core promoter and the basal transcriptional machinery. *Dev. Biol.* **339**, 225–229 (2010).
- Hubmann, G., Thevelein, J. M. & Nevoigt, E. Natural and modified promoters for tailored metabolic engineering of the yeast *Saccharomyces cerevisiae*. *Methods Mol. Biol.* **1152**, 17–42 (2014).
- Sun, J. et al. Cloning and characterization of a panel of constitutive promoters for applications in pathway engineering in *Saccharomyces cerevisiae*. *Biotechnol. Bioeng.* **109**, 2082–2092 (2012).
- Tirosh, I. & Barkai, N. Two strategies for gene regulation by promoter nucleosomes. *Genome Res.* **18**, 1084–1091 (2008).
- Rando, O. J. & Winston, F. Chromatin and transcription in yeast. *Genetics* **190**, 351–387 (2012).

56. Redden, H. & Alper, H. S. The development and characterization of synthetic minimal yeast promoters. *Nat. Commun.* **6**, 7810 (2015).
57. Curran, K. A. et al. Short synthetic terminators for improved heterologous gene expression in yeast. *ACS Synth. Biol.* **4**, 824–832 (2015).
58. Blazeck, J. et al. Controlling promoter strength and regulation in *Saccharomyces cerevisiae* using synthetic hybrid promoters. *Biotechnol. Bioeng.* **109**, 2884–2895 (2012).
59. Lee, T. J. et al. Suppression of expression between adjacent genes within heterologous modules in yeast. *G3 (Bethesda)* **4**, 109–116 (2014).
60. Weiner, A. et al. High-resolution nucleosome mapping reveals transcription-dependent promoter packaging. *Genome Res.* **20**, 90–100 (2010).
61. Hodges, C. et al. Nucleosomal fluctuations govern the transcription dynamics of RNA polymerase II. *Science* **325**, 626–628 (2009).
62. Lublinier, S., Keren, L. & Segal, E. Sequence features of yeast and human core promoters that are predictive of maximal promoter activity. *Nucleic Acids Res.* **41**, 5569–5581 (2013).
63. Raveh-Sadka, T., Levo, M. & Segal, E. Incorporating nucleosomes into thermodynamic models of transcription regulation. *Genome Res.* **19**, 1480–1496 (2009).
64. Raveh-Sadka, T. et al. Manipulating nucleosome disfavoring sequences allows fine-tune regulation of gene expression in yeast. *Nat. Genet.* **44**, 743–750 (2012).
65. Sharon, E. et al. Probing the effect of promoters on noise in gene expression using thousands of designed sequences. *Genome Res.* **24**, 1698–1706 (2014).
66. Sharon, E. et al. Inferring gene regulatory logic from high-throughput measurements of thousands of systematically designed promoters. *Nat. Biotechnol.* **30**, 521–530 (2012).
67. Lykke-Andersen, S., Mapendano, C. K. & Jensen, T. H. An ending is a new beginning: transcription termination supports re-initiation. *Cell Cycle* **10**, 863–865 (2011).
68. Shandilya, J. & Roberts, S. G. The transcription cycle in eukaryotes: from productive initiation to RNA polymerase II recycling. *Biochim. Biophys. Acta* **1819**, 391–400 (2012).
69. Grzechnik, P., Tan-Wong, S. M. & Proudfoot, N. J. Terminate and make a loop: regulation of transcriptional directionality. *Trends Biochem. Sci.* **39**, 319–327 (2014).
70. Curran, K. A. et al. Use of expression-enhancing terminators in *Saccharomyces cerevisiae* to increase mRNA half-life and improve gene expression control for metabolic engineering applications. *Metab. Eng.* **19**, 88–97 (2013).
71. Ito, Y. et al. Characterization of five terminator regions that increase the protein yield of a transgene in *Saccharomyces cerevisiae*. *J. Biotechnol.* **168**, 486–492 (2013).
72. Morse, N. J. et al. Yeast terminator function can be modulated and designed on the basis of predictions of nucleosome occupancy. *ACS Synth. Biol.* **6**, 2086–2095 (2017).
73. Wei, L. et al. Characterization of terminators in *Saccharomyces cerevisiae* and an exploration of factors affecting their strength. *ChemBioChem* **18**, 2422–2427 (2017).
74. Yamanishi, M. et al. A genome-wide activity assessment of terminator regions in *Saccharomyces cerevisiae* provides a ‘terminatome’ toolbox. *ACS Synth. Biol.* **2**, 337–347 (2013).
75. Yamanishi, M., Katahira, S. & Matsuyama, T. TPS1 terminator increases mRNA and protein yield in a *Saccharomyces cerevisiae* expression system. *Biosci. Biotechnol. Biochem.* **75**, 2234–2236 (2011).
76. Song, W. et al. Can terminators be used as insulators into yeast synthetic gene circuits? *J. Biol. Eng.* **10**, 19 (2016).
77. Yarger, J. G., Armilei, G. & Gorman, M. C. Transcription terminator-like element within a *Saccharomyces cerevisiae* promoter region. *Mol. Cell. Biol.* **6**, 1095–1101 (1986).
78. Flagfeldt, D. B. et al. Characterization of chromosomal integration sites for heterologous gene expression in *Saccharomyces cerevisiae*. *Yeast* **26**, 545–551 (2009).
79. Dai, Z. & Dai, X. Nuclear colocalization of transcription factor target genes strengthens coregulation in yeast. *Nucleic Acids Res.* **40**, 27–36 (2012).
80. Berger, A. B. et al. High-resolution statistical mapping reveals gene territories in live yeast. *Nat. Methods* **5**, 1031–1037 (2008).
81. Duan, Z. et al. A three-dimensional model of the yeast genome. *Nature* **465**, 363–367 (2010).
82. Donczew, R. & Hahn, S. Mechanistic differences in transcription initiation at TATA-less and TATA-containing promoters. *Mol. Cell. Biol.* **38**, e00448–17 (2018).
83. Verdone, L. et al. Chromatin remodeling during *Saccharomyces cerevisiae* ADH2 gene activation. *Mol. Cell. Biol.* **16**, 1978–1988 (1996).
84. Kalderon, D. et al. A short amino acid sequence able to specify nuclear location. *Cell* **39**, 499–509 (1984).
85. Dvir, S. et al. Deciphering the rules by which 5'-UTR sequences affect protein expression in yeast. *Proc. Natl. Acad. Sci. USA* **110**, E2792–E2801 (2013).
86. Wang, M., Li, S. & Zhao, H. Design and engineering of intracellular-metabolite-sensing/regulation gene circuits in *Saccharomyces cerevisiae*. *Biotechnol. Bioeng.* **113**, 206–215 (2016).
87. Teo, W. S. & Chang, M. W. Bacterial XylRs and synthetic promoters function as genetically encoded xylose biosensors in *Saccharomyces cerevisiae*. *Biotechnol. J.* **10**, 315–322 (2015).
88. Stanton, B. C. et al. Genomic mining of prokaryotic repressors for orthogonal logic gates. *Nat. Chem. Biol.* **10**, 99–105 (2014).
89. Brophy, J. A. & Voigt, C. A. Principles of genetic circuit design. *Nat. Methods* **11**, 508–520 (2014).
90. Andrews, L. B., Nielsen, A. A. K. & Voigt, C. A. Cellular checkpoint control using programmable sequential logic. *Science* **361**, eaap8987 (2018).
91. Auslander, D. et al. Programmable full-adder computations in communicating three-dimensional cell cultures. *Nat. Methods* **15**, 57–60 (2018).
92. Goentoro, L. et al. The incoherent feedforward loop can provide fold-change detection in gene regulation. *Mol. Cell* **36**, 894–899 (2009).
93. Kuttykrishnan, S. et al. A quantitative model of glucose signaling in yeast reveals an incoherent feed forward loop leading to a specific, transient pulse of transcription. *Proc. Natl. Acad. Sci. USA* **107**, 16743–16748 (2010).
94. Sheff, M. A. & Thorn, K. S. Optimized cassettes for fluorescent protein tagging in *Saccharomyces cerevisiae*. *Yeast* **21**, 661–670 (2004).
95. Lam, A. J. et al. Improving FRET dynamic range with bright green and red fluorescent proteins. *Nat. Methods* **9**, 1005–1012 (2012).
96. Nagai, T. et al. A variant of yellow fluorescent protein with fast and efficient maturation for cell-biological applications. *Nat. Biotechnol.* **20**, 87–90 (2002).
97. Mumberg, D., Muller, R. & Funk, M. Yeast vectors for the controlled expression of heterologous proteins in different genetic backgrounds. *Gene* **156**, 119–122 (1995).
98. Blount, B. A. et al. Rational diversification of a promoter providing fine-tuned expression and orthogonal regulation for synthetic biology. *PLoS ONE* **7**, e33279 (2012).
99. Guldener, U. et al. A new efficient gene disruption cassette for repeated use in budding yeast. *Nucleic Acids Res.* **24**, 2519–2524 (1996).
100. Goldstein, A. L., Pan, X. & McCusker, J. H. Heterologous URA3MX cassettes for gene replacement in *Saccharomyces cerevisiae*. *Yeast* **15**, 507–511 (1999).
101. Holstege, F. C. et al. Dissecting the regulatory circuitry of a eukaryotic genome. *Cell* **95**, 717–728 (1998).
102. Wapinski, I. et al. Natural history and evolutionary principles of gene duplication in fungi. *Nature* **449**, 54–61 (2007).
103. Kaplan, N. et al. The DNA-encoded nucleosome organization of a eukaryotic genome. *Nature* **458**, 362–366 (2009).
104. McLaughlin, J. A. et al. SynBioHub: a standards-enabled design repository for synthetic biology. *ACS Synth. Biol.* **7**, 682–688 (2018).
105. Madsen, C. et al. Synthetic Biology Open Language (SBOL) version 2.3. *J. Integr. Bioinform.* **16**, 20190025 (2019).
106. Bilibchenko, L. et al. Eugene—a domain specific language for specifying and constraining synthetic biological parts, devices, and systems. *PLoS ONE* **6**, e18882 (2011).

## Acknowledgements

This work was supported by funding from the US Department of Energy (DE-SC0018368 to Y.C. and C.A.V.), NSF Synthetic Biology Engineering Research Center (SA5284-11210 to C.A.V.), NSF award (1522074 to D.D.), US Defense Advanced Research Projects Agency 1KMR award (HR0011-12-C-0067 to C.A.V.) and SD2 (FA8750-17-C-0229 to S.Z. and C.A.V.), as well as a research contract from DSM (to E.M.Y.). Cello testing and feedback were provided by C. Myers and students at the University of Utah.

## Author contributions

Y.C. and C.A.V. conceived the study and designed the experiments. S.Z. performed the computational work. E.M.Y. cloned and characterized native yeast parts. T.J. and D.D. designed and developed Cello 2.0. Y.C. performed all of the other experiments and analysed the data. Y.C., E.M.Y. and C.A.V. wrote the manuscript.

## Competing interests

The authors declare no competing interests.

## Additional information

**Extended data** is available for this paper at <https://doi.org/10.1038/s41564-020-0757-2>.

**Supplementary information** is available for this paper at <https://doi.org/10.1038/s41564-020-0757-2>.

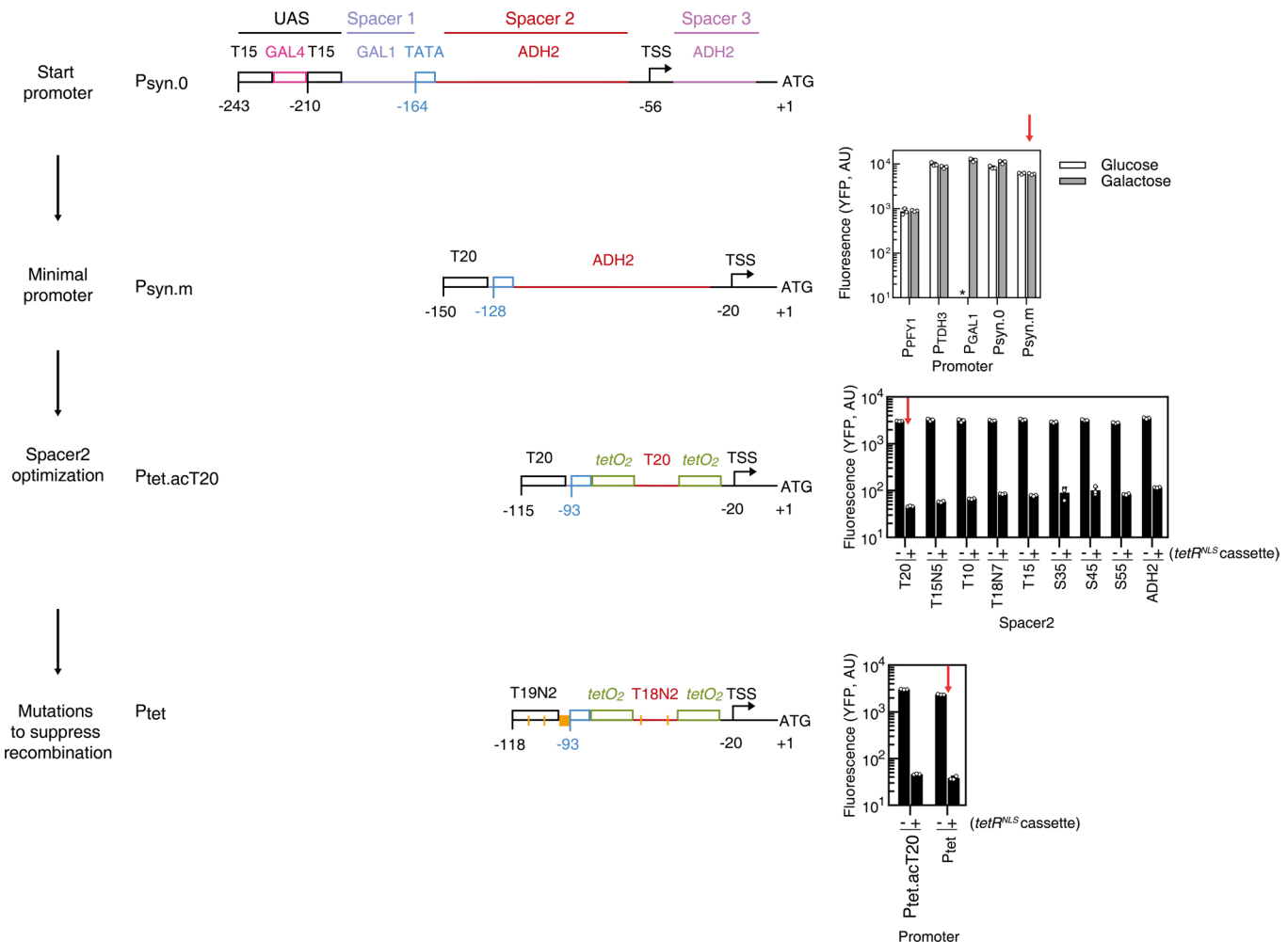
**Correspondence and requests for materials** should be addressed to C.A.V.

**Peer review information** Peer reviewer reports are available.

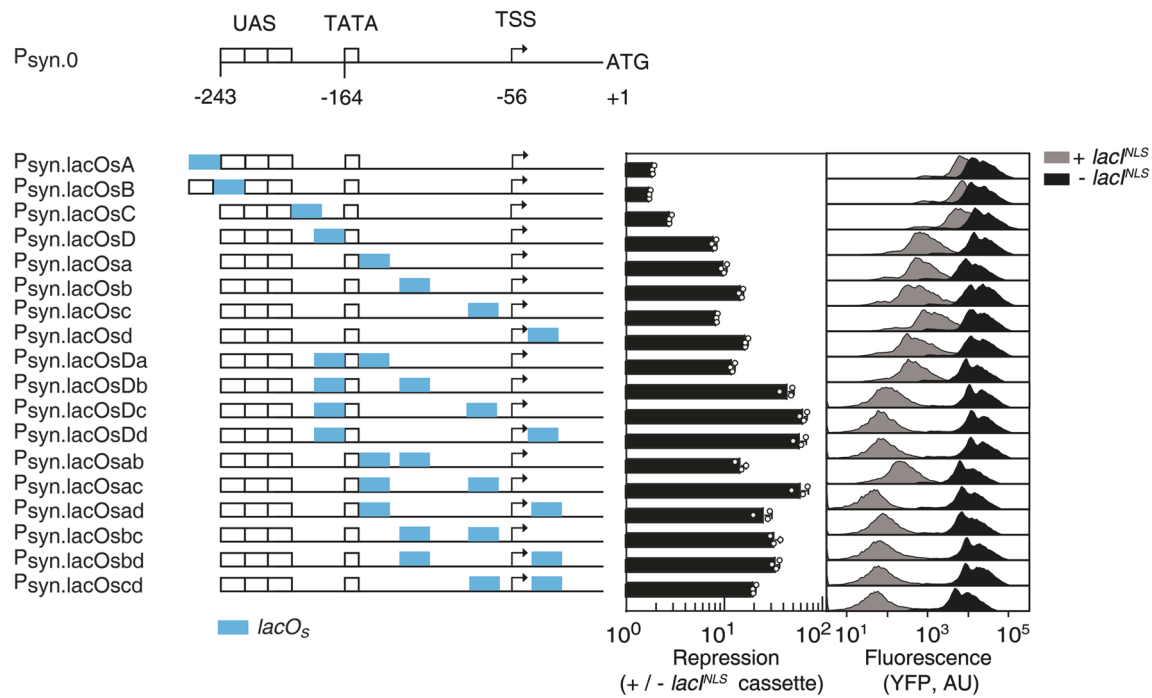
**Reprints and permissions information** is available at [www.nature.com/reprints](http://www.nature.com/reprints).

**Publisher's note** Springer Nature remains neutral with regard to jurisdictional claims in published maps and institutional affiliations.

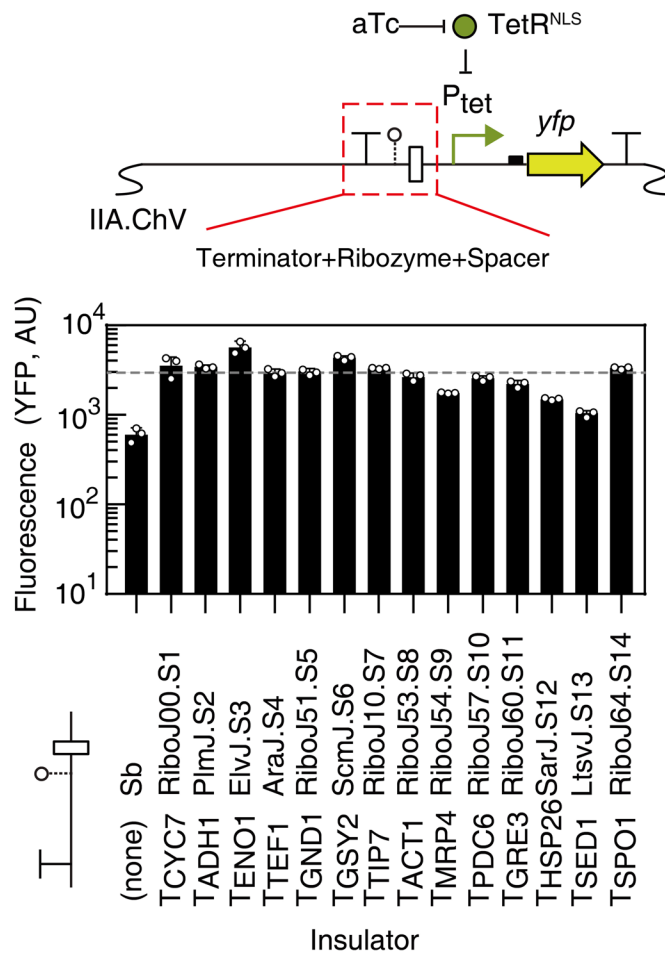
© The Author(s), under exclusive licence to Springer Nature Limited 2020



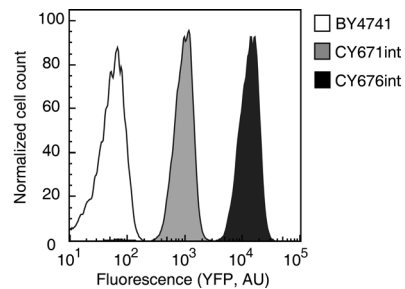
**Extended Data Fig. 1 | Optimization steps for building the TetR-responsive minimal promoter.** The annotated promoter sequences are provided in Supplementary Table 5, including intermediates, and all part sequences are provided in Supplementary Table 10. The promoters are evaluated through the transcriptional fusion with *yfp* and this cassette is carried on a plasmid (Supplementary Figure 15). The data are measured under identical experimental conditions (Methods). In the top graph, the carbon source is either 2% glucose or 2% galactose. The star indicated that there is no fluorescence detected over background. When TetR<sup>NLS</sup> is expressed from a second plasmid (Supplementary Figure 15), this is indicated by “+tetR<sup>NLS</sup> cassette”. The red arrows show the data corresponding to the promoter selected for the next round of optimization. The horizontal orange lines mark where mutations are made in order to diversify the part sequence to avoid homologous recombination in the context of a circuit. The data represent the average of three experiments performed on different days. The optimizations steps for other promoters are shown in Supplementary Figs. 2–12.



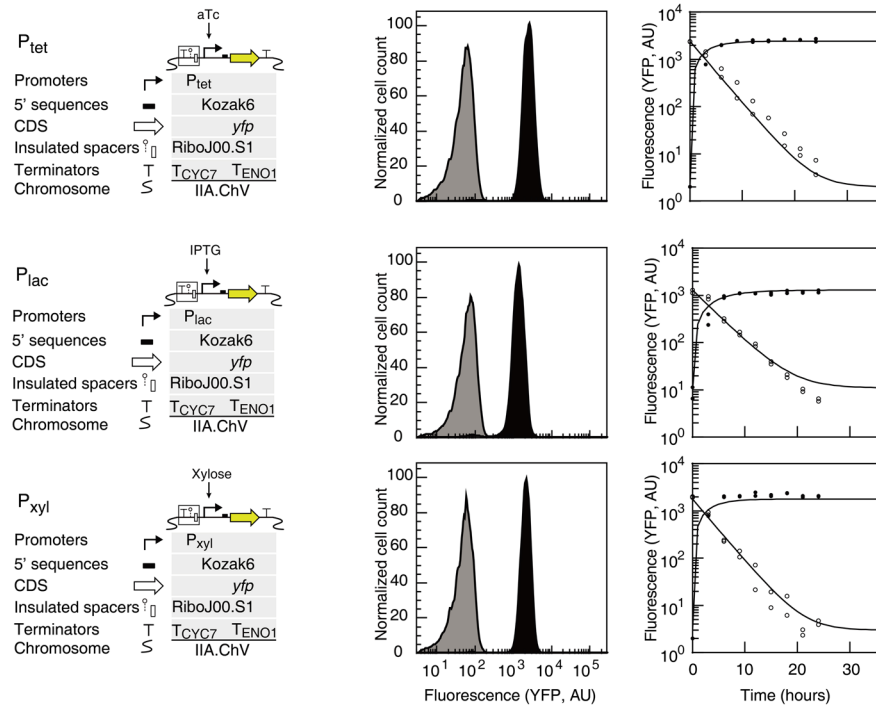
**Extended Data Fig. 2 | Promoter designs with varying lacO<sub>s</sub> operator spacing.** The sequences of genetic parts are provided in Supplementary Table 5. The UAS binds to Gal4 and the TSS is a 20bp sequence from ADH2 (Extended Data Figure 1). The promoters are transcriptionally fused to *yfp* and cloned into a plasmid backbone (Supplementary Figure 15). A second plasmid is constructed where LacI is expressed from a constitutive promoter (Supplementary Figure 15). The cytometry distributions show the fluorescence from the reporter plasmid in the absence (black) and presence (grey) of the LacI plasmid and the reported “Repression” is the ratio of the medians of these distributions. The data represent the average of three experiments performed on different days.



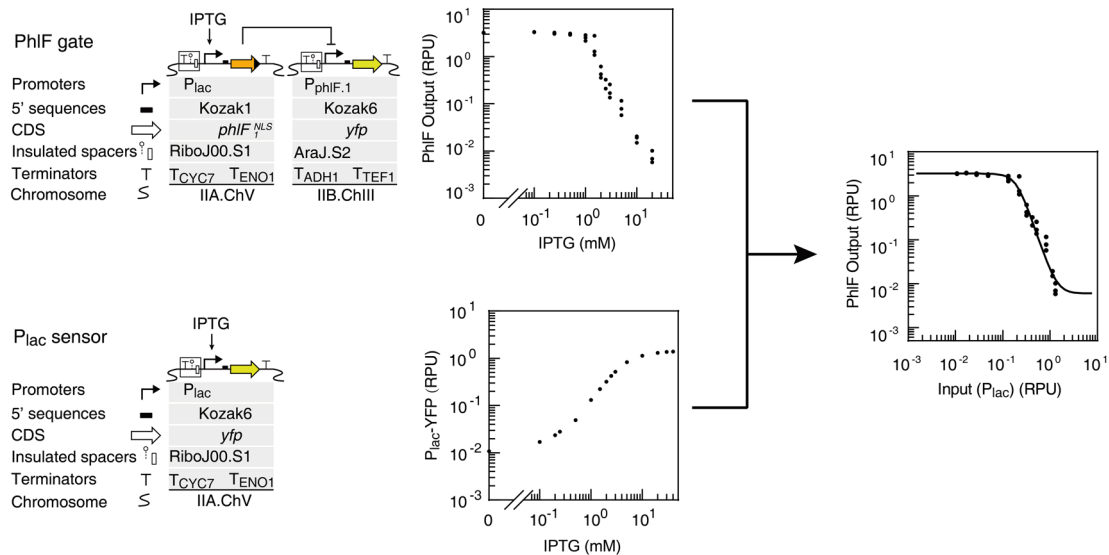
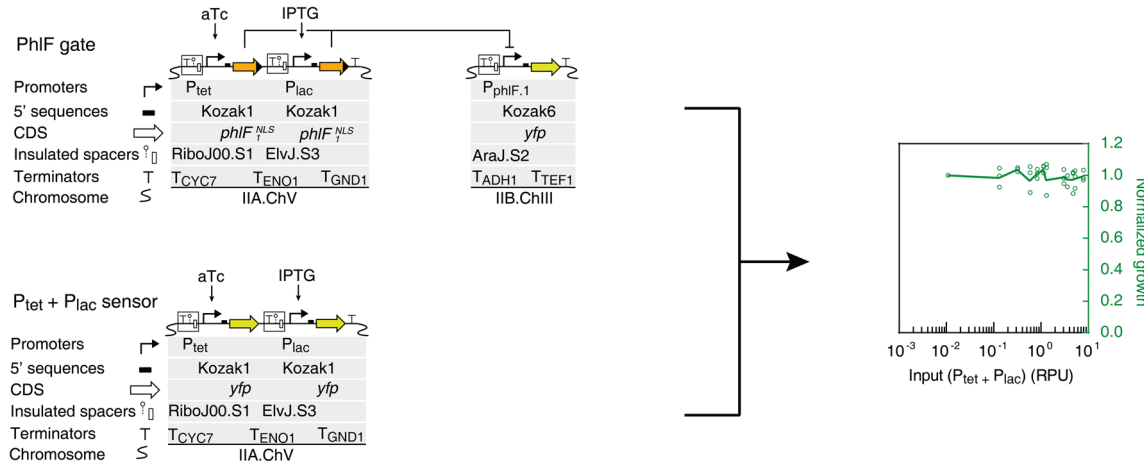
**Extended Data Fig. 3 | Upstream insulator impact on an inducible promoter.** The fluorescence values are shown when P<sub>tet</sub> is maximally induced (100 ng/ml). Sb is a 450bp nonfunctional DNA sequence. When there is no insulator (none)-Sb, then the maximum expression is lower. The horizontal dashed line is the average of the fluorescence measurements from the strains containing an insulator. The strains are described in Supplementary Table 4 and insulator sequences are provided in Supplementary Table 5. The data represent the average of three experiments performed on different days.



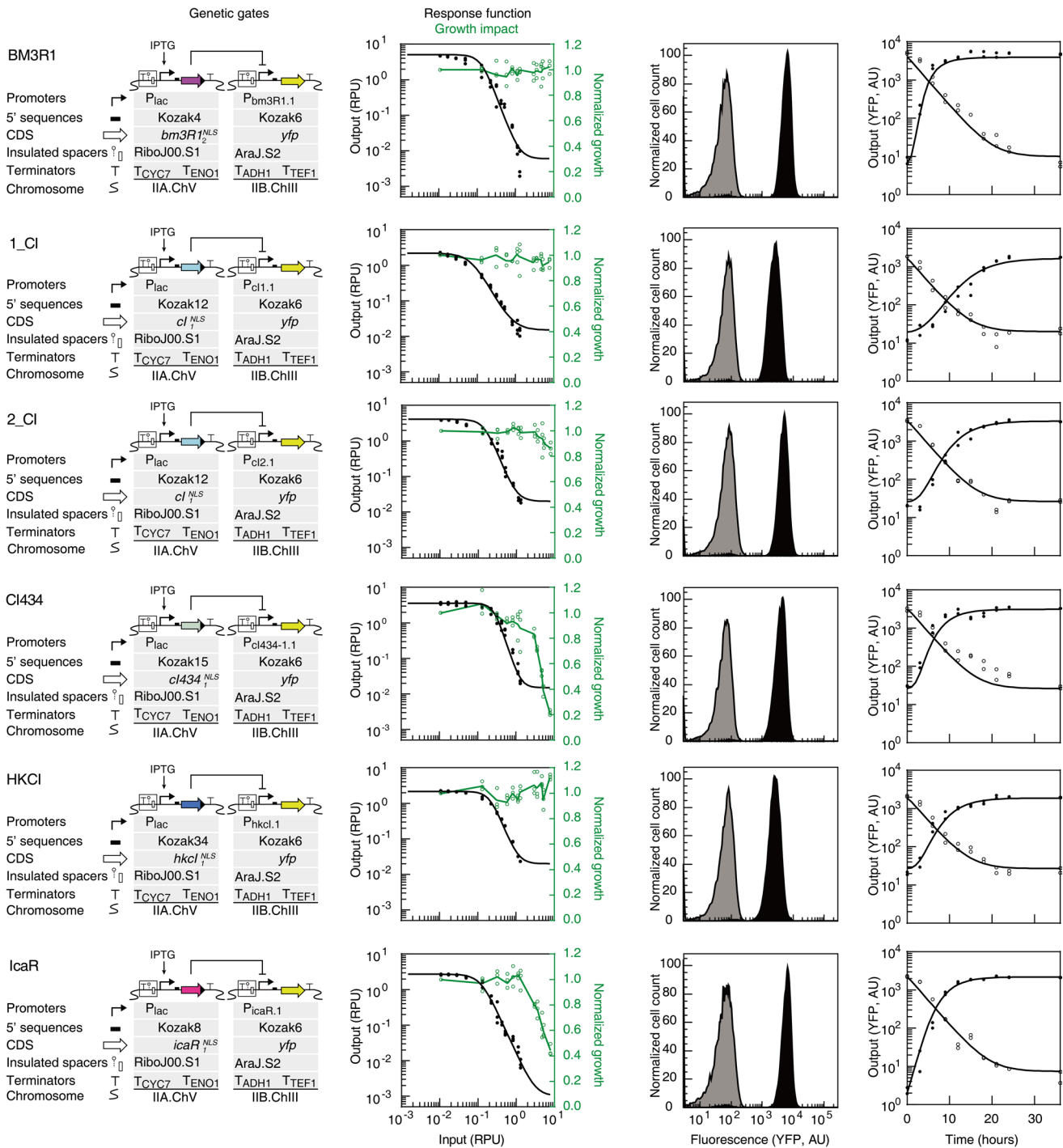
**Extended Data Fig. 4 | Cytometry distribution for the RPU reference standard.** The cytometry distributions show the fluorescence from the strain containing the RPU standard (*S. cerevisiae* CY671int) (grey), *S. cerevisiae* BY4741 cells (white) and a reporter strain containing the strong native promoter  $P_{TDH3}$  (*S. cerevisiae* CY676int) (black). Detailed strain information is provided in Supplementary Tables 3 and 8. Three experiments were repeated on different days with similar results.



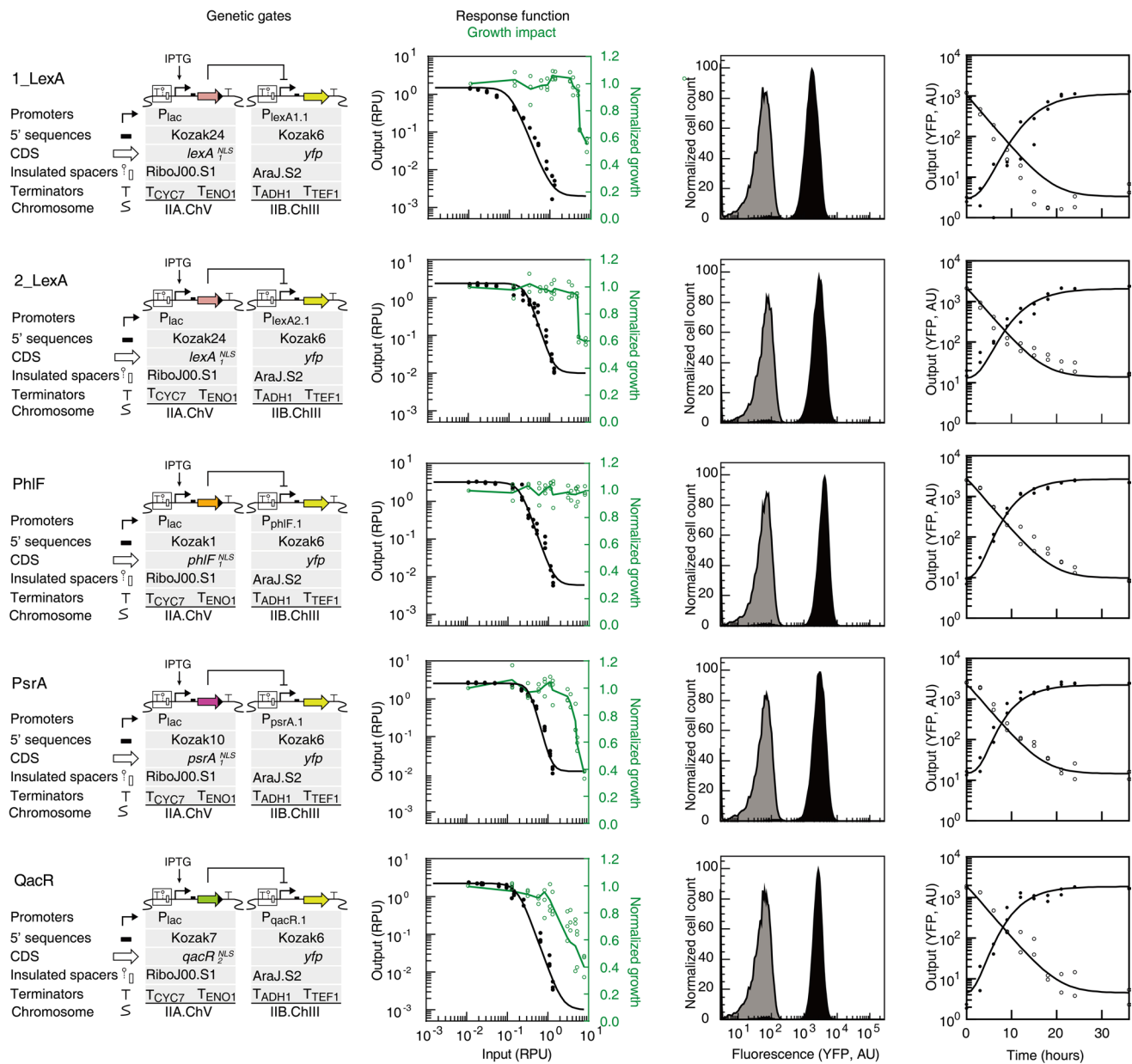
**Extended Data Fig. 5 | Sensor cytometry distributions and sensor dynamics.** These data correspond to Fig. 4d and Supplementary Table 1. The detailed schematic for the reporter of each sensor shown to the left and the corresponding strains are provided in Supplementary Table 4. The sequences for the genetic parts are provided in Supplementary Tables 4 and 8. The experimental conditions are as described in the Methods. Two representative cytometry distributions are shown when cells containing the sensors are grown in (0 or 100 ng/ml) aTc, (0 or 20 mM) IPTG, or (0 or 10 mM) xylose. The dynamic data was measured as described in the Methods and fit to Equations 4 and 5. The data points combine two experiments performed on different days.

**a****b**

**Extended Data Fig. 6 | Converting the x-axis of a NOT gate response function to RPU.** **a**, An example is shown to demonstrate how data gathered using two strains are combined to create a NOT gate response function. The PhIF gate is strain *S. cerevisiae* CY960-CY663int and the IPTG sensor is strain *S. cerevisiae* CY639int (Supplementary Table 4). Both strains are evaluated by adding different concentrations of IPTG (left to right): 0.0, 0.1, 0.2, 0.5, 1.0, 1.5, 2.0, 2.5, 3.0, 5.0, 10 and 20 mM. The growth conditions, cytometry measurements, and normalization to RPU are described in the Methods. The graph to the right is built using the RPU measurements for the input promoter ( $P_{lac}$ ) and output promoter ( $P_{phIF.1}$ ) at each inducer concentration. The data are then fit to Equation 2, the parameters for which are presented in Supplementary Table 2. **b**, Growth impacts are processed similarly so that the x-axis can be reported as promoter activity and not inducer concentration. As an example, the growth impact of the PhIF gate (*S. cerevisiae* CY1085-CY663int) is shown along with the strain used to determine the activity of the ( $P_{tet}$  +  $P_{lac}$ ) promoters. The strains were induced with 0, 1, 3, 5, 7.5, 10, 20 mM IPTG (0 ng/ml aTc) or 1, 2.5, 5, and 20 mM IPTG (100ng/ml aTc). The data represent three experiments performed on different days.

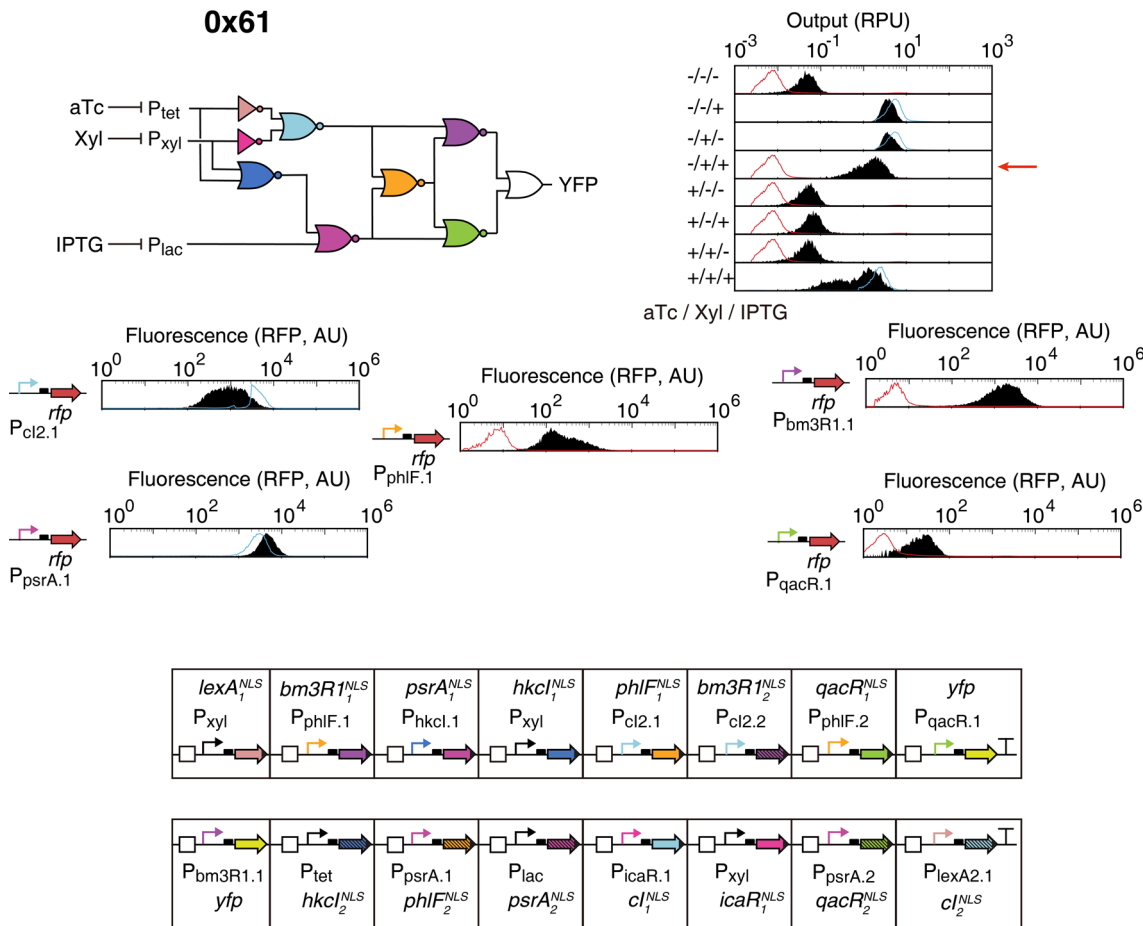


**Extended Data Fig. 7 | Detailed characterization of the NOT gates.** These data correspond to Fig. 5b and Supplementary Table 2. The detailed schematic for the gate is shown to the left and the corresponding strains are provided in Supplementary Table 4. The sequences for the genetic parts are provided in Supplementary Tables 4 and 8. The data used to fit the response functions (Equation 2) were calculated as described in Extended Data Figure 6 and the resulting parameters are provided in Supplementary Table 2. The data represent three experiments performed on different days. The experimental conditions are as described in the Methods. Two representative cytometry distributions are shown when cells containing the gates are grown in 0 or 20 mM IPTG. The dynamic data was measured as described in the Methods and fit to Equations 6, 7 and 8. The data represent two experiments performed on different days.

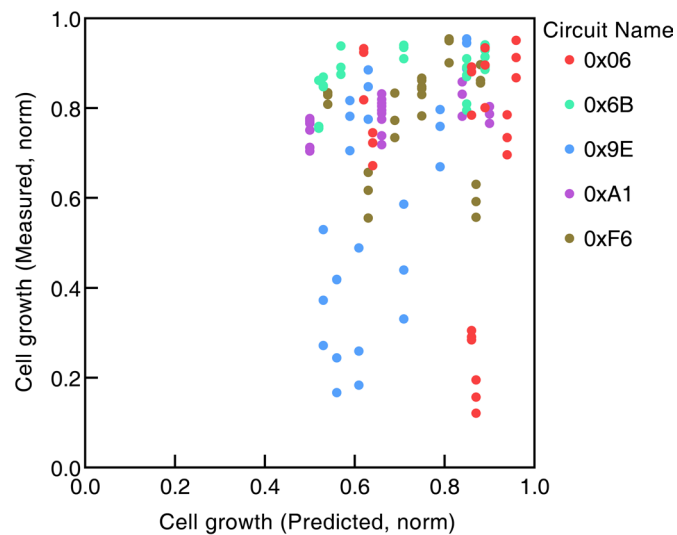


**Extended Data Fig. 8 | Detailed characterization of the NOT gates.** These data correspond to Fig. 5b and Supplementary Table 2. The detailed schematic for the gate is shown to the left and the corresponding strains are provided in Supplementary Table 4. The sequences for the genetic parts are provided in Supplementary Tables 4 and 8. The data used to fit the response functions (Equation 2) were calculated as described in Extended Data Figure 6 and the resulting parameters are provided in Supplementary Table 2. The data represent three experiments performed on different days. The experimental conditions are as described in the Methods. Two representative cytometry distributions are shown when cells containing the gates are grown in 0 or 20 mM IPTG. The dynamic data was measured as described in the Methods and fit to Equations 6, 7 and 8. The data represent two experiments performed on different days.

0x61



**Extended Data Fig. 9 | The failure of the 0x61 circuit.** The logic diagram is shown with gate colors corresponding to the assigned repressor. The response of the circuit is shown for different combinations of inducer: 100ng/ml aTc, 10mM xylose, and 20mM IPTG. The experimental data are shown as cytometry distributions (black) and blue/red distributions show the ON/OFF output predicted by Cello. The states behave as predicted, except for the -/+/- state, which should be OFF but is measured as being ON. To determine where this breakage originates the output promoters of intermediate gates are fused to *rfp* and inserted at the HO locus. The measured responses are then compared to those predicted. The population variability in the response of the CI gate, which causes errors that propagate to the final BM3R1 gate. The DNA sequence of the circuit is provided in Supplementary Table 11, the strains are provided in Supplementary Table 4, and the reporter constructs in Supplementary Table 4. Three experiments were repeated on different days with similar results.



**Extended Data Fig. 10 | The impact on growth from carrying the circuits in different states.** Each point represents a different combination of inducers for a given circuit. The prediction is made using Cello and is calculated by multiplying the empirically-measured growth impact of all the gates with input promoter activities corresponding to that state [7]. Details regarding the growth assay are presented in the Methods and normalized to *S. cerevisiae* BY4741 in the same growth conditions. The data represent three experiments performed on different days.

# Reporting Summary

Nature Research wishes to improve the reproducibility of the work that we publish. This form provides structure for consistency and transparency in reporting. For further information on Nature Research policies, see [Authors & Referees](#) and the [Editorial Policy Checklist](#).

## Statistics

For all statistical analyses, confirm that the following items are present in the figure legend, table legend, main text, or Methods section.

n/a Confirmed

- The exact sample size ( $n$ ) for each experimental group/condition, given as a discrete number and unit of measurement
- A statement on whether measurements were taken from distinct samples or whether the same sample was measured repeatedly
- The statistical test(s) used AND whether they are one- or two-sided  
*Only common tests should be described solely by name; describe more complex techniques in the Methods section.*
- A description of all covariates tested
- A description of any assumptions or corrections, such as tests of normality and adjustment for multiple comparisons
- A full description of the statistical parameters including central tendency (e.g. means) or other basic estimates (e.g. regression coefficient) AND variation (e.g. standard deviation) or associated estimates of uncertainty (e.g. confidence intervals)
- For null hypothesis testing, the test statistic (e.g.  $F$ ,  $t$ ,  $r$ ) with confidence intervals, effect sizes, degrees of freedom and  $P$  value noted  
*Give P values as exact values whenever suitable.*
- For Bayesian analysis, information on the choice of priors and Markov chain Monte Carlo settings
- For hierarchical and complex designs, identification of the appropriate level for tests and full reporting of outcomes
- Estimates of effect sizes (e.g. Cohen's  $d$ , Pearson's  $r$ ), indicating how they were calculated

*Our web collection on [statistics for biologists](#) contains articles on many of the points above.*

## Software and code

Policy information about [availability of computer code](#)

Data collection

BD FACS DIVA software was used to collect all of the cytometry data in this study. A multi-mode microplate reader (Biotek, Synergy 526 H1) was used for the data collection.

Data analysis

FlowJo version 10.4.1 (TreeStar Inc.) was used to analyze the cytometry data. MATLAB R2018b were used for simulating dynamics. MATLAB scripts were available at <https://github.com/VoigtLab>. Cello2.0 was available at [cellocad.org](http://cellocad.org). Cello2.0 codes were available at <https://github.com/CIDARLAB/Cello-v2>.

For manuscripts utilizing custom algorithms or software that are central to the research but not yet described in published literature, software must be made available to editors/reviewers. We strongly encourage code deposition in a community repository (e.g. GitHub). See the Nature Research [guidelines for submitting code & software](#) for further information.

## Data

Policy information about [availability of data](#)

All manuscripts must include a [data availability statement](#). This statement should provide the following information, where applicable:

- Accession codes, unique identifiers, or web links for publicly available datasets
- A list of figures that have associated raw data
- A description of any restrictions on data availability

Genetic parts and the UCF file SC1C1G1T1.UCF are available as Supplementary Information. Source data for Figs. 2–7 are in this article. The data that support the findings of this study are available from the corresponding author upon reasonable request. Plasmids and cloning strains generated in this study will be available on Addgene ([https://www.addgene.org/Christopher\\_Voigt/](https://www.addgene.org/Christopher_Voigt/)) and the corresponding author on request.

# Field-specific reporting

Please select the one below that is the best fit for your research. If you are not sure, read the appropriate sections before making your selection.

Life sciences       Behavioural & social sciences       Ecological, evolutionary & environmental sciences

For a reference copy of the document with all sections, see [nature.com/documents/nr-reporting-summary-flat.pdf](http://nature.com/documents/nr-reporting-summary-flat.pdf)

## Life sciences study design

All studies must disclose on these points even when the disclosure is negative.

Sample size	Statistical methods were not used to predetermine sample size. Sample size was determined to be adequate based on experimental consistency and effect, generally 3 independent replicates on different days.
Data exclusions	No data were excluded from the manuscript
Replication	All attempts at replication were successful. We performed the experiments on three days.
Randomization	Randomization was not used in this study
Blinding	Blinding was not used in this study

## Reporting for specific materials, systems and methods

We require information from authors about some types of materials, experimental systems and methods used in many studies. Here, indicate whether each material, system or method listed is relevant to your study. If you are not sure if a list item applies to your research, read the appropriate section before selecting a response.

### Materials & experimental systems

n/a	Involved in the study
<input checked="" type="checkbox"/>	<input type="checkbox"/> Antibodies
<input type="checkbox"/>	<input checked="" type="checkbox"/> Eukaryotic cell lines
<input checked="" type="checkbox"/>	<input type="checkbox"/> Palaeontology
<input checked="" type="checkbox"/>	<input type="checkbox"/> Animals and other organisms
<input checked="" type="checkbox"/>	<input type="checkbox"/> Human research participants
<input checked="" type="checkbox"/>	<input type="checkbox"/> Clinical data

### Methods

n/a	Involved in the study
<input checked="" type="checkbox"/>	<input type="checkbox"/> ChIP-seq
<input type="checkbox"/>	<input checked="" type="checkbox"/> Flow cytometry
<input checked="" type="checkbox"/>	<input type="checkbox"/> MRI-based neuroimaging

## Eukaryotic cell lines

Policy information about [cell lines](#)

Cell line source(s)      Saccharomyces cerevisiae Strain BY4741 from EUROSCARF

Authentication      We confirmed all integrations by PCR and DNA sequencing.

Mycoplasma contamination      Yeast cell doesn't have this contamination.

Commonly misidentified lines  
(See [ICLAC](#) register)      No common misidentified lines were used.

## Flow Cytometry

### Plots

Confirm that:

- The axis labels state the marker and fluorochrome used (e.g. CD4-FITC).
- The axis scales are clearly visible. Include numbers along axes only for bottom left plot of group (a 'group' is an analysis of identical markers).
- All plots are contour plots with outliers or pseudocolor plots.
- A numerical value for number of cells or percentage (with statistics) is provided.

## Methodology

Sample preparation	Yeast cells were diluted in either PBS with cycloheximide
Instrument	BD LSR II Fortessa running based on FACSDIVA software
Software	FACS Diva software for collection; FlowJo for data analysis.
Cell population abundance	Typical samples contained 20,000 or more cells.
Gating strategy	Cells in mid-log phase were gated as >500 SSA and >500 FSA to remove cellular debris. We also gated for un-budded cells by SSW and FSW.

Tick this box to confirm that a figure exemplifying the gating strategy is provided in the Supplementary Information.